

**INVESTIGATING CELL ADHESION VIA PARALLEL DISK ROTATIONAL
FLOW: A BIOCOMPATIBILITY STUDY**

A Thesis

by

ARACELY ROCHA

Submitted to the Office of Graduate Studies of
Texas A&M University
in partial fulfillment of the requirements for the degree of

MASTER OF SCIENCE

December 2008

Major Subject: Mechanical Engineering

**INVESTIGATING CELL ADHESION VIA PARALLEL DISK ROTATIONAL
FLOW: A BIOCOMPATIBILITY STUDY**

A Thesis

by

ARACELY ROCHA

Submitted to the Office of Graduate Studies of
Texas A&M University
in partial fulfillment of the requirements for the degree of

MASTER OF SCIENCE

Approved by:

Chair of Committee,	Hong Liang
Committee Members,	Jaime Grunlan
	Zoubeida Ounaies
Head of Department,	Dennis O'Neal

December 2008

Major Subject: Mechanical Engineering

ABSTRACT

Investigating Cell Adhesion via Parallel Disk Rotational Flow: A

Biocompatibility Study. (December 2008)

Aracely Rocha, B.S., The University of Texas-Pan American

Chair of Advisory Committee: Dr. Hong Liang

The major impact of this research lies in the aspect of improved design and long term biocompatibility of materials used for implants. There are two goals in this research. The first goal is to develop a methodology to quantitatively measure cell-material adhesion. The second goal is to obtain fundamental understanding of cell-material adhesion mechanisms. A rotating parallel disk is used to measure cell adhesion. The rotational system applies a controlled shear stress to the cultured cells. The shear stress experienced by the cells varies with radial location, being highest at the edge and zero at the disk's center. There is a critical point along the radius where the shear stress experienced by the cells equals their adhesion strength. The cells outside it are removed and the cells inside it remain attached to the surface.

NIH 3T3 Swiss mouse fibroblasts and chick retina neuron cells from 6-day embryos are used in this study. The fibroblasts were cultured on poly(methyl methacrylate) (PMMA), polycarbonate (PC), and on gold coated poly(vinylidene fluoride) (Au/PVDF). The critical shear stress for fibroblasts was the lowest for PC with 5.09 dynes/cm² and highest for PMMA with 21.0 dynes/cm². This four-fold difference is

mainly due to the chemical structure of PMMA which promotes higher cell adhesion when compared to PC.

Neurons were cultured on poly-D-lysine coated glass to promote cell adhesion. The critical shear stress of neuron cells varied from 3.94 to 27.8 dynes/cm² these values are directly proportional to the applied shear stress. The neuron adhesion plateau at ~27 dynes/cm² which indicates the maximum adhesion strength of the neuron/poly-D-lysine coated glass pair.

This thesis contains six chapters. Chapter I describes the importance of cell adhesion for biocompatibility. Chapter II describes in more detail the goals of this research and the expected results. Chapter III lists all the materials, equipment, and methods used in this study. The most significant results are summarized in Chapter IV. The observations and results obtained are explained in detail in Chapter V and Chapter VI describes the key outcomes as well as proposes questions for the advancement of this research.

ACKNOWLEDGEMENTS

I would like to thank my committee chair, Dr. Liang, for her guidance and support throughout the course of this research and to my committee members, Dr. Grunlan and Dr. Ounaies for their advice and time.

I would also like to thank Dr. Maria Hahn, Dr. Gladys Ko and Dr. Kuihuan Jian for their support in cell culture experiments. Thanks also go to the members of the Surface Science Group for their help, ideas, and great support at each group presentation.

I want to extend my gratitude to the NSF- Bridge to the Doctorate Fellowship, especially to Shannon Henderson, for their financial support and encouragement. I would also like to thank National Science Foundation (grant number 0535578) and the associated IREE (International Research and Education in Engineering) for their partial financial support that made this work possible.

Finally, thanks to my husband for his patience, understanding, love, and support.

NOMENCLATURE

ASTM	American Society for Testing and Materials
NIH	National Institutes of Health
FDA	Food and Drug Administration
ISO	International Organization for Standardization
ECM	Extra Cellular Matrix
PDL	Poly-D-Lysine
AFM	Atomic Force Microscope
PMMA	Poly(methyl methacrylate)
PS	Polystyrene
PCL	poly ϵ -caprolactone
PLLA	poly(L-lactide)
PLGA	poly(lactic-co-glycolic acid)
PC	Polycarbonate
PBS	Phosphate buffered saline solution
PVDF	Polyvinylidene Fluoride
UHMWPE	Ultra high molecular weight polyethylene
RS-100	Ceramic fiber reinforced alumina composite
Si	Silicon
NiCu	Nickel copper
Ag	Silver

Au	Gold
ω	Angular velocity
μ	viscosity
H	Distance between disks (gap)
τ_a	applied shear stress for testing
τ_c	Calculated critical shear stress = cell adhesion strength
ρ	density
R_a	Average surface roughness
R	Spindle or rotating disk radius
r	Radial axis
R_c	Critical radius. Equivalent to cell adhesion strength.
F_L	Lateral force
F_N	Normal force
Re	Reynolds number
\vec{v}	velocity vector
SEM	Scanning electron microscope
p	pressure gradient
g	gravitational acceleration

TABLE OF CONTENTS

	Page
ABSTRACT	iii
ACKNOWLEDGEMENTS	v
NOMENCLATURE.....	vi
TABLE OF CONTENTS	viii
LIST OF FIGURES.....	x
LIST OF TABLES	xiv
 CHAPTER	
I INTRODUCTION.....	1
1.1. Background	1
1.2. Importance of cell adhesion	3
1.2.1. Cell adhesion proteins.....	4
1.2.1.1. Fibronectin	6
1.2.1.2. Poly-d-lysine	7
1.3. Measuring cell adhesion.....	7
1.3.1. Single cell adhesion tests	8
1.3.2. Cell network adhesion tests	11
II MOTIVATION AND OBJECTIVES	15
III EXPERIMENTS	18
3.1. Materials.....	18
3.1.1. Cell culture.....	18
3.1.1.1. Cells.....	18
3.1.1.2. Cell preparation and activation	21
3.1.1.3. Culture media	22
3.1.1.4. Substrates for cell culture.....	23
3.1.1.5. Cell culture dishware.....	24
3.1.2. Materials for testing.....	24
3.1.3. Cell fixatives.....	24

CHAPTER	Page
3.2. Equipment	25
3.2.1. Imaging equipment	25
3.2.2. Cell culture equipment.....	26
3.2.3. Surface measuring equipment.....	27
3.2.4. Rheometer	28
3.2.5. Surface cleaning and cell storage.....	29
3.3. Methods.....	29
3.3.1. Cell cultures	29
3.3.1.1. Solutions for fibroblast culture.....	29
3.3.1.2. Fibroblast culture substrates.....	30
3.3.1.3. Fibroblast culture.....	31
3.3.1.4. Prepare fibroblast samples for imaging.....	33
3.3.1.5. Solutions for neuron culture.....	33
3.3.1.6. Neuron culture substrates.....	33
3.3.1.7. Neuron culture.....	34
3.3.1.8. Prepare neuron samples for imaging.....	35
3.3.2. Testing conditions.....	35
IV RESULTS.....	37
4.1. NIH 3T3 Swiss mouse fibroblasts.....	37
4.2. Chick embryo retina neurons	42
V MECHANISMS OF CELL ADHESION.....	49
5.1. Analysis of parallel disk rotational flow	49
5.2. Critical shear stress.....	55
5.3. Effects of cell elasticity on R_c and τ_c	64
5.4. Effect of substrate material on R_c and τ_c	67
VI CONCLUSIONS.....	72
6.1. Future recommendations	75
REFERENCES.....	76
APPENDIX A	83
VITA	84

LIST OF FIGURES

	Page
Figure 1 Structure of an amino acid, the protein building block.....	5
Figure 2 The four levels of protein structure [1].	5
Figure 3 Structure of fibronectin molecule [1].	6
Figure 4 Building block of poly-D-lysine.	7
Figure 5 Measuring cell adhesion with AFM. The AFM tip measures the force necessary to pull the cell from the substrate [29].	9
Figure 6 Measuring cell adhesion with a modified AFM. The cantilever is used to shear the cell from the surface [31].	9
Figure 7 Measuring cell adhesion with a pipette. The sphere on top is the target material and the cell is the sphere at the bottom [32].	10
Figure 8 Diagram of shear flow systems used to study the adhesion of cells on external substrates.	11
Figure 9 Endothelial cells adhesion study as a function of static and shear stress after 3 hours of cell seeding [26].	12
Figure 10 Parallel disk rotational flow diagram. The flow is generated on the media by rotating the top plate.	13
Figure 11 Test objectives. Cells are cultured on substrate and tested with parallel rotating disk to generate a shear flow.	17
Figure 12 3T3 Swiss mouse fibroblast originally extracted by Todaro and Green. Image by Nikon MicroscopyU [47].	19
Figure 13 3T3 mouse fibroblasts at 3 days of culture on 2, 6 Bis(3 amino phenoxybenzo nitrile) (β -CN APB) at 10X magnification with an Axiovert A200 inverted transmission microscope (Carl Zeiss).	19
Figure 14 Bipolar neurons extracted from the retina of 6day chick embryos taken after 5 days of culture. Courtesy of Dr. Subrata Kundu.	20

	Page
Figure 15 Bipolar neuron cells from 6-day chick retina cultured on PDL coated glass with 1000X under a VHX-600 3D digital microscope (Keyence Microscope).	21
Figure 16 Carl Zeiss inverted transmission microscope (Axiovert 200). Image from Carl Zeiss [56]......	25
Figure 17 VHX-600 3D microscope from Keyence.	26
Figure 18 JEOL JSM-6400 Scanning Electron Microscope in the Microscopy & Imaging Center at Texas A&M University [57]......	26
Figure 19 Cell culture incubator from Lab Line.	27
Figure 20 TR200 Profilometer from Qulitest.....	27
Figure 21 Diagram of parallel plate rotational rheometer with basic components.....	28
Figure 22 AR-G2 Rheometer from TA Instruments.	28
Figure 23 Experimental set up. The cell cultured substrate is secured to the lower disk.....	36
Figure 24 SEM images of $R_a = 0.636\mu\text{m}$ of PMMA_25_03. The imaging points are shown in 2g. The line scale is equivalent to $30\mu\text{m}$	41
Figure 25 $R_c = 0.70\text{ cm}$ for Au/PVDF_20_01. Image obtained with Axiovert inverted transmission microscope.....	42
Figure 26 SEM images of $R_a = 1.05\text{ cm}$ for PC_10_01. The imaging points are shown in 2g. The line scale is equivalent to $30\mu\text{m}$	42
Figure 27 $R_c=1.158\text{cm}$ for S15_10. With VHX-600 Keyence microscope. The scale bar indicates $500\mu\text{m}$	44
Figure 28 $R_c=0.976\text{cm}$ for S16_25. With VHX-600 Keyence microscope. The scale bar indicates $500\mu\text{m}$	45
Figure 29 $R_c=0.663\text{cm}$ for S17_40. With VHX-600 Keyence microscope. The scale bar indicates $500\mu\text{m}$	45
Figure 30 $R_c=0.631\text{cm}$ for S19_55. With VHX-600 Keyence microscope. The scale bar indicates $500\mu\text{m}$	45

	Page
Figure 31 $R_c=0.483\text{cm}$ for S20_70. With VHX-600 Keyence microscope. The scale bar indicates $500\mu\text{m}$	46
Figure 32 $R_c=0.933\text{cm}$ for S24_25. With VHX-600 Keyence microscope. The scale bar indicates $500\mu\text{m}$	46
Figure 33 $R_c=0.394\text{cm}$ for S25_30. With VHX-600 Keyence microscope. The grid is $50\mu\text{m}/\text{div}$	46
Figure 34 Results of chick neurons on PDL coated glass. The R_C is inversely proportional to τ_a	47
Figure 35 The instability introduced by the free energy at the PBS/air interface depends on the shape of the fluid (PBS).....	51
Figure 36 Reynolds number throughout test for S15_10. This shows the Re increases with time.	53
Figure 37 Difference in viscosity for sample of PMMA tested with and without cells at $\tau_a=25\text{ dynes}/\text{cm}^2$	54
Figure 38 Schematic of parallel disk rotational flow in cylindrical coordinates (r, θ, z). The total gap is H and the maximum radius is R	56
Figure 39 Results of chick embryo neurons on poly-D-lysine coated glass with traditional flow analysis.....	58
Figure 40 Viscosity vs. shear strain of PBS during S25_30 test. The changing viscosity with shear strain indicates PBS is not Newtonian.	59
Figure 41 Angular velocity vs. test time of PBS during S25_30 test. The ω approaches a constant value.....	59
Figure 42 Results of chick embryo neurons on poly-D-lysine coated glass with simplified equation.	61
Figure 43 Comparison of traditional flow analysis and simplified flow analysis for 3T3 fibroblasts.	62
Figure 44 Comparison of traditional flow analysis and simplified flow analysis for chick embryo neuron samples.....	63
Figure 45 Schematic of normal (F_N) and lateral forces (F_L) acting on an attached cell.	65

	Page
Figure 46 Steps for cell detachment when exposed to a shear flow.	66
Figure 47 Images of S16_25 before and after testing. Cell shape and density inside the Rc was not affected by the shear flow.....	66
Figure 48. The poly-D-lysine proteins show alignment after testing in the flow direction.....	67
Figure 49 Reaction mechanisms for fibronectin and PMMA.	70

LIST OF TABLES

	Page
Table 1 Cell-cell and cell-substrate adhesion studies where the adhesion strength of only one cell is measured.	10
Table 2 Adhesion studies between cell network and substrate.	14
Table 3 Components of Eagle's medium.	22
Table 4 Materials used as substrates for cell culture experiments.	23
Table 5 Test conditions for NIH 3T3 Swiss mouse fibroblasts.	38
Table 6 NIH 3T3 Swiss mouse fibroblasts samples damaged before testing.	39
Table 7 3T3 Swiss mouse fibroblasts samples damaged after testing.	40
Table 8 The NIH 3T3 Swiss mouse fibroblasts shear strength adhesion.	41
Table 9 Test conditions for chick embryo neuron cells.	43
Table 10 Results of chick embryo neuron cells on poly-D-lysine coated glass substrates.	44
Table 11 Reynolds number for test procedure used in NIH 3T3 Swiss mouse fibroblasts.	52
Table 12 Reynolds number for test procedure used in chick embryo retina neurons.	52
Table 13 The τ_c of NIH 3T3 Swiss mouse fibroblast on various surfaces.	57
Table 14 The τ_c of chick embryo neuron cells on poly-d-Lysine coated glass.	57
Table 15 The τ_c of 3T3 fibroblast on various surfaces with proposed analysis.	61
Table 16 The τ_c of chick neuron cells on PDL coated glass with proposed analysis.	61
Table 17 The % difference between traditional and proposed analyses for 3T3 fibroblast.	62
Table 18 The % difference between traditional and proposed analyses for chick neurons on PDL coated glass.	63

	Page
Table 19 The average surface roughness (Ra) of materials.	68
Table 20 Chemical structure of the polymers used as substrates for NIH 3T3 Swiss mouse fibroblast cultures.....	69

CHAPTER I

INTRODUCTION

Advances in materials science have led to the development of a wide variety of materials to be used in the body, such as implants. Nevertheless, the biocompatibility of the materials and cells remain to be critical for successful and long lasting implants. The key to address the issue of compatibility lies in the fundamental aspects of cell adhesion. Cell adhesion is essential for normal cell communication and function and it plays an important role in defining the shape of the tissues it forms. When a foreign material is introduced to the body, like an artificial implant, cell function is greatly affected if cell adhesion to the surface is changed. This chapter provides necessary background of cells and cell adhesion followed by a thorough review of the state-of-art techniques used in cell-adhesion measurements.

1.1. Background

Appropriate cell adhesion to biomaterials is an important aspect of biocompatibility. Biomaterials are used in a wide variety of applications including sensors, artificial implants, wound treating, and drug delivery systems [1-3] to name a few. The degree of biocompatibility required for any material depends on its application. A material used for artificial joints requires good cell adhesion and must stay in the body for an extended period of time. On the other hand, a material used for wound treating should promote cell reproduction and is only in contact with the skin for a short period

This thesis follows the style of *Biorheology*.

of time. The American Society for Testing and Materials (ASTM), the National Institutes of Health (NIH), the Food and Drug Administration (FDA), and the International Organization for Standardization (ISO) have specific guidelines for testing materials for potential bioapplications [1-3]. With the increase of applications and available materials, assessing biocompatibility is a critical point in the design and development of materials and devices for biological applications. Biocompatibility is defined as the ability of a system or component to perform its intended design with no undesirable effects while preventing local and systematic responses in the host [2, 4]. Because of the wide variety of applications, the development of a single test to assess biocompatibility is a challenging task.

Materials must follow a thorough examination to assess their biocompatibility before they can be introduced to the body. The tests are divided in four phases. The first phase consists of studying the physical, chemical, and biological properties of the material. Phase two is designed to assess the biocompatibility of the material. The in vitro tests that must be performed in this phase are specific to the application. These tests must simulate the conditions the material will have to withstand in the body and analyzes its durability as well as its positive or negative effect on the body. Phase three is designed to verify the material processing and how this affects the end result. Finally, phase four consists of carrying in vivo tests along with monitoring of the implanted systems [1, 2]. Biomaterial applications are classified as: surface contact devices, communication devices, and long term implant devices [2, 3]. An artificial joint is an example of a long-term implant device. Good cell adhesion is critical in long term

implant devices since the device is expected to stay in the body without affecting its function for over 20 years.

1.2. Importance of cell adhesion

Cell adhesion is considered the single most important aspect of cytotoxicity [5] because it mediates cell-cell and cell-substrate interaction [3, 6-11], cell shape, and cell function [3, 5, 7-9, 11, 12]. Cytotoxicity tests are conducted to understand how materials affect cell growth, shape, function, and adhesion. Cytotoxicity tests consist of exposing the material to live cells and biofluids that would surround it in the body. The live tissue or biofluids are closely examined to verify for signs of damage caused by the material and/or its byproducts [1-3, 5]. Measuring the adhesion strength between the cells and a biomaterial is the most reliable and desirable method to assess biocompatibility in vitro. If the adhesion between the cells and the implant is equal or similar to those present in the body, it is an indication that the material is suitable for the application and cell function will not be greatly affected. Therefore, understanding how biomaterials affect cell response and behavior, independent of the material's potential application, is a critical aspect of biocompatibility.

In order to allow easier handling of tissues, it is separated into its individual cells by chemical and mechanical processes. The separated cells are called a cell culture. The cell culture is placed on the material and it is carefully observed under controlled environmental conditions (temperature, humidity, and %CO₂ concentration) for a given period of time. Obtaining a cell culture is a critical process since cell behavior and function must not be affected. Extensive behavior and characterization tests are

conducted to cell cultures before they are used for in-vitro cytotoxicity evaluation. The cultured cells, because they are no longer protected by the extra cellular matrix (ECM), are maintained in culture media which is made of proteins and antibiotics [5]. Two common cell cultures used for in vitro tests are fibroblast and neurons. Fibroblasts are connective cells found around other highly organized structural tissues and organs. Neurons are cells of the nervous system that send information to the brain through electrochemical processes [13, 14].

1.2.1. Cell adhesion proteins

Cell attachment is mediated by the extracellular matrix (ECM), which is made of polysaccharides (sugars) and collagen (proteins) that provide structural support and protection to cells. The proteins in the ECM are also responsible for carrying all necessary electrochemical processes and control tissue elasticity, humidity, and adhesion [14, 15] and are key elements in the cell/biomaterial interface [1].

Proteins are made up of amino acids and are made of one carboxyl group (COOH), one amino group (H₂N), one hydrogen atom (H), and one functional group (R). Figure 1 shows the structure of the amino acids. The functional group dictates whether the amino acid is non-polar, polar, positively charged, or negatively charged [1, 14, 15]. The H₂N group of one amino acid reacts with the COOH of another to form proteins [1]. The structure of proteins is similar to that of polymers. Protein chains are long and can be highly coiled with some branching (like an amorphous polymer) and are also able to form highly oriented molecules (similar to crystalline polymers).

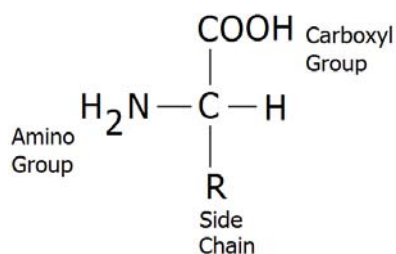


Figure 1 Structure of an amino acid, the protein building block.

The structural arrangement of proteins can be described in four levels as shown in Figure 2. The primary structure considers the connection between amino acids; analogous to the chain growth in polymers. The secondary structure is due to weaker hydrogen bonds within the molecules causing the protein chain to coil and form a helix. The tertiary structure represents the 3D arrangement of a single protein chain while the quaternary structure refers to the interaction between different protein chains [1, 15].

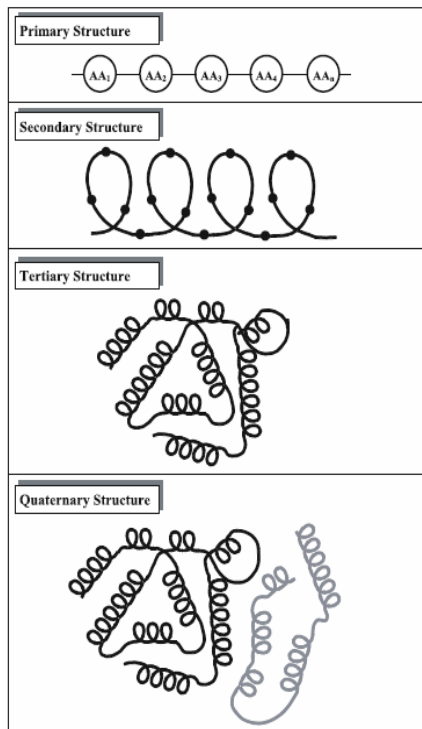


Figure 2 The four levels of protein structure [1].

The proteins that participate in cell-cell adhesion and cell-substrate adhesion vary by cell type. In the case of fibroblasts, cytokines are the main proteins that mediate cell-cell adhesion and fibronectin is the main protein that controls cell-substrate adhesion in the ECM [12, 16-18]. Bipolar neuron cells need the assistance of poly-d-lysine (PDL), a synthetic protein, to attach to an external surface [13].

1.2.1.1. Fibronectin

Fibronectin is the most studied adhesion molecule, although many others participate in the cell-substrate adhesion of fibroblasts. It is found in bone, skin, and connective tissues and it is made of two linear chains of fibrin, collagen, and heparin (all amino acids). The chains are connected at one end with disulfide bonds and have carboxylic ends; this is the side that bonds to the cells. The opposite ends of the fibronectin chains have amide groups. The molecular weight of fibronectin is typically 220,000 Daltons [1]. Figure 3 shows the structure and components of fibronectins. The two chains are connected by disulfide bonds and have carboxylic ends that attach to the cell. The opposite ends have amide groups which attach to the material's surface.

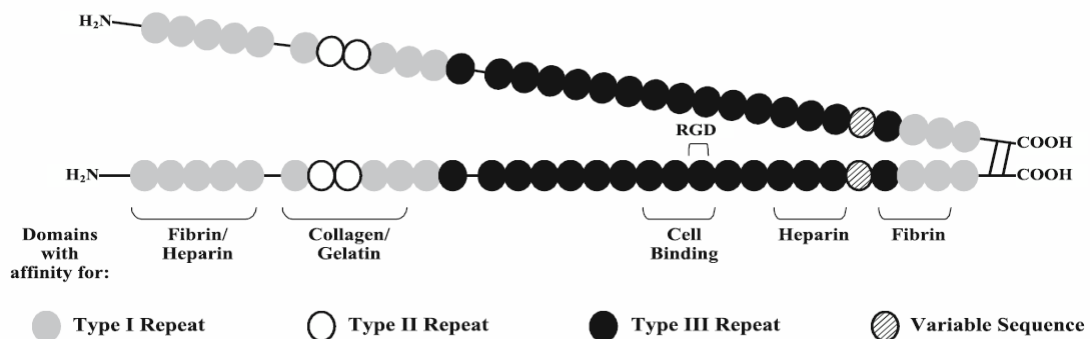


Figure 3 Structure of fibronectin molecule [1].

1.2.1.2. Poly-d-lysine

Poly-D-lysine (PDL) is an artificial protein designed to promote neuron adhesion to any surfaces. It is engineered to promote cell adhesion without affecting normal cell function. Figure 4 is the amino acid that forms poly-d-lysine. The amide group (NH₂) of one amino acid reacts with the alcohol (OH) of another to polymerize and forms water (H₂O) as a byproduct of the reaction [19]. Since this is an engineered protein, it can be manufactured to any desired length.

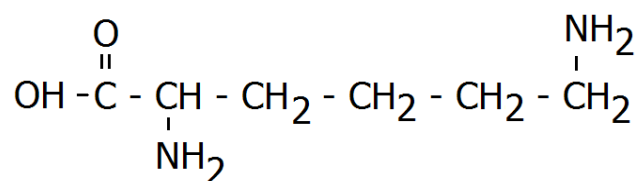


Figure 4 Building block of poly-D-lysine.

Proteins have one electropositive and one electronegative end. In general, the negative side attaches to the cell and the positive end attaches to the material. Therefore, electronegative surfaces help promote cell adhesion and cell proliferation.

1.3. Measuring cell adhesion

Cell adhesion is the main factor that controls cell function, the main aspect of cytotoxicity and a key element of material biocompatibility. Cell adhesion to foreign surfaces is a fundamental factor when studying a material's biocompatibility. Several methods to assess cell-cell and cell-substrate adhesion have been developed but are only designed to provide qualitative results [17, 20-22]. However, quantitative results, like

adhesion strength, provide a better comparison of the biocompatibility of every material and of any surface-treated material [6-9, 12, 18, 20, 23, 24].

Previous works on cell adhesion were performed to assess other aspects of cell-biomaterial interaction and are not always focused on studying the biocompatibility of the materials. The work of Bushman et al., Ono et al., and Reutelingsperger et al. addresses the effect of blood flow on the adhesion of endothelial cells to the interior walls of arteries, veins, and blood vessels [25-27]. Their observations are focused on % cell adhesion to internal walls as a function of shear flow and time. LaPlaca and Thibault studied the effect of impact in a collision on the communication of neural systems [28]. The methods developed to measure cell adhesion strength to a surface can be divided in two general groups: single cell and cell network measurements.

1.3.1. **Single cell adhesion tests**

In a single cell adhesion test, the adhesion strength is measured by attaching or detaching a single cell from the substrate with an atomic force microscope (AFM) or by micromanipulation with a pipette. An AFM or a modified AFM is used to measure the force required to pull [29, 30] or shear [12, 31] one cell from the substrate. Benoit et al. used an AFM to measure the required force to separate a single cell from the substrate [29]. This measuring system has been used for a variety of cell lines and materials. Figure 5 demonstrates Benoit's and colleagues work and it is an example of an AFM used to measure the force required to separate a cell from the surface. Figure 6 shows the work of Sagvolden and colleagues; they used a modified AFM tip used to measure the force required to shear one cell from the surface.

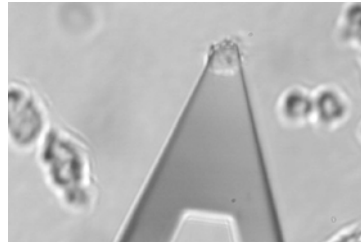


Figure 5 Measuring cell adhesion with AFM. The AFM tip measures the force necessary to pull the cell from the substrate [29].

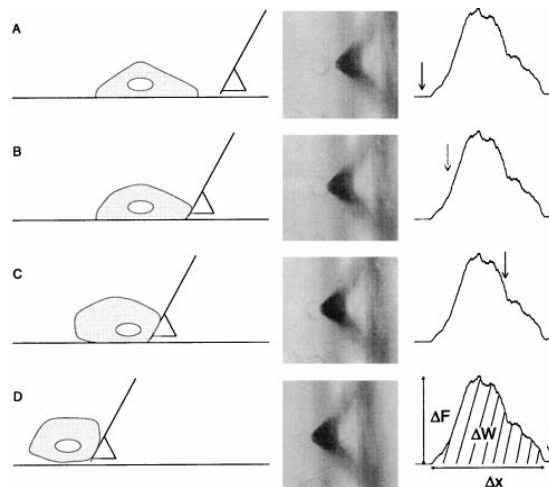


Figure 6 Measuring cell adhesion with a modified AFM. The cantilever is used to shear the cell from the surface [31].

Shao and Hochmuth measured the force necessary to separate a single cell from a plastic bead with a pipette. The plastic bead (top sphere), have a larger diameter than the pipette opening and is held under vacuum. They measured the required vacuum pressure to pull the cell from the bead as shown in Figure 7 [32]. Table 1 summarizes some of the single-cell adhesion measurements previously performed along with the adhesion strength.

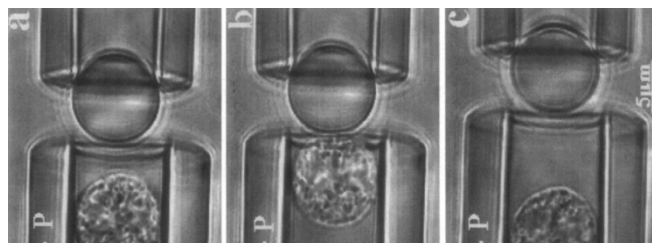


Figure 7 Measuring cell adhesion with a pipette. The sphere on top is the target material and the cell is the sphere at the bottom [32].

Table 1 Cell-cell and cell-substrate adhesion studies where the adhesion strength of only one cell is measured.

Year [Ref]	Test Summary	Cell	Substrate	Adhesion
1999 [31]	Modified AFM to measure cell-substrate adhesion	NHIK3025 carcinoma	Hydrophilic and hydrophobic PS	Maximum 204 nN
2000 [12]	Modified AFM to shear cells with cantilever	L929 murine fibroblast	Glass, PS, and fibronectin (F) and collagen (C) coated PS	Glass=300nN PS = 300nN F-coated =550nN C-coated=900nN
2000 [29]	AFM to measure cell-cell adhesion	Dictyostelium discoideum cells	csA glycoprotein coated glass	23±8pN
2003 [20]	Micropipette manipulation. Pull force at 8,12,24 h, &5 days	Pig chondrocytes	PCL, PLLA, PLGA polymers	At 5 days PCL=45nN PLLA=41nN PLGA=55
2006 [30]	AFM to measure cell-nanoparticle substrate adhesion	L929 fibroblast, Caco2 human colon cancer, B16F10	Silica nanoparticles	L929 @ 4d=12nN, Caco2 @ 10d=2nN, B16F10 @4d=10nN
2006 [6]	AFM to measure cell-cell adhesion	WM115 melanoma cells	Human umbilical cord endothelial cells	48 ±7pN

Although single cell adhesion tests are effective methods to measure cell adhesion, materials for bioapplications requires the interaction of the material with tissue or a cell network instead of a single cell. Therefore, measuring the adhesion of a cell network on a material provides a better representation of the tissue response to a material.

1.3.2. Cell network adhesion tests

The most common method for analyzing the average cell adhesion strength on a material involves the application of defined levels of shear stress. The average cell adhesive force is generally taken to be the shear force at which the majority of cells are removed from the surface. Four different methods for shear stress testing have been reported syringing [33, 34], centrifugation [18, 23, 35], channel flow [22, 36, 37], and rotational flow which includes rotational flow between cone and plates [25, 37-40], between parallel disks [26, 28], or rotational flow over a plate [9, 27]. Figure 8 shows the four most common methods. The red arrows indicate plate motion and the black arrows indicate flow motion.

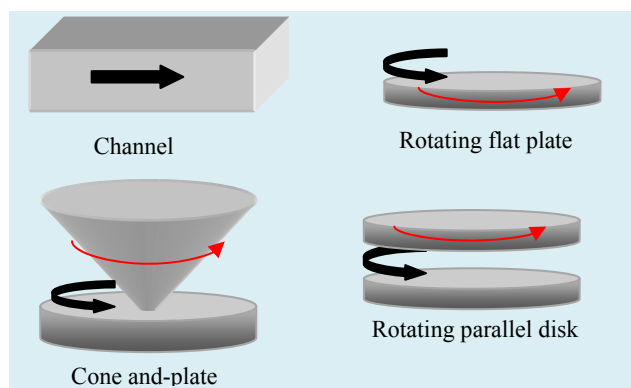


Figure 8 Diagram of shear flow systems used to study the adhesion of cells on external substrates.

Adhesion studies by syringing, centrifugation, channel flow, rotating flat plate, and cone and plate rotational flow have only been used to provide qualitative results of remnant cells on the surface after shear flow exposure. The results are usually reported as % cells remaining on the surface versus applied shear stress and do not provide the actual cell-substrate adhesion strength. In the cone and plate rotational flow systems the applied shear stress depends on the radius and the cone angle [25, 37-39] and for parallel rotational disk it depends on distance between plates and distance from center.

Ono et al. used the rotating parallel disk to study how shear flow affects the adhesion mechanisms of endothelial cells. Endothelial cells line the internal walls of veins and arteries. They observed the how cells adhered to surfaces under a controlled shear flow. The system was designed to feed cells into the rotating flow and counting the % cells that attached to the surface after a given time period, from 3 hours up to 8 days [26]. The results obtained by Ono et al. are summarized in Figure 9. These results are qualitative and do not provide the cell adhesion strength.

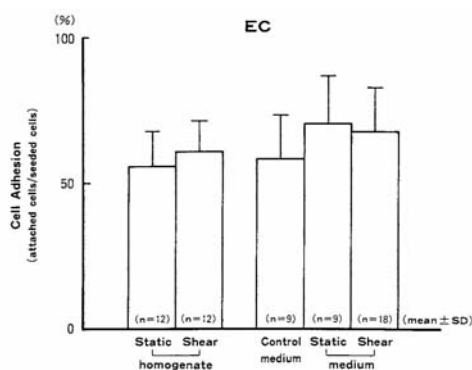


Figure 9 Endothelial cells adhesion study as a function of static and shear stress after 3 hours of cell seeding [26].

LaPlaca et al. applied the rotating parallel disk system to observe the effect of impact on neuron cells. A diagram of this system is illustrated in Figure 10. The flow was used to simulate an impact injury. The shear flow was introduced as a pulse, high shear flow for a short time period (only fractions of a second). Their observations were focused on observing how an impact affected neuron elasticity and communication. Neuron elasticity was assessed by measuring the strain [28].

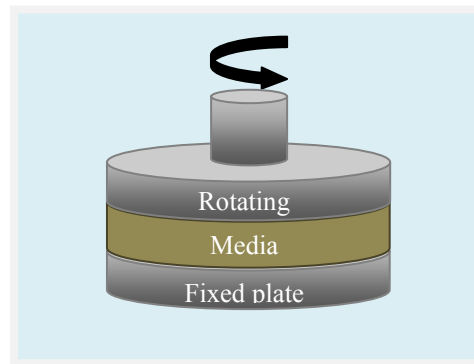


Figure 10 Parallel disk rotational flow diagram. The flow is generated on the media by rotating the top plate.

Rotational flow systems are the most widely used method to study cell behavior under a shear flow [37]. The parallel disk rotating system has been used to study many aspects of the cell including cell communication and their ability to attach to a surface when exposed to a shear flow. The work of Ono et al. and LaPlaca et al. demonstrate the system is suitable for multiple cell lines since they worked on endothelial and neural cells respectively [26, 28].

Table 2 summarizes some of the cell adhesion studies performed between a cell network to various substrates. In general, tests are generally performed with shear flow and the results are qualitative because they only present the percent number of cells that

remain on the surface after hours or days. Specific details about the cell type and substrate are also given. It is important to note that the shear values reported indicate the shear stress at which 0% of cells are attached to the surface.

Table 2 Adhesion studies between cell network and substrate.

Year [Ref]	Test Summary	Cell	Substrate	Results
1986 [17]	No shear flow	Human fibroblasts	Fibronectin coated glass	Maximum 80% cell adhesion
1989 [18]	Shear flow by centrifugal force	NIL cell fibroblasts	Fibronectin (F) & Tenascin (T) coated glass	$F = \max 40 \text{ dynes}/_{\text{cell}} \times 10^{-5}$ $T = \max 2 \text{ dynes}/_{\text{cell}} \times 10^{-4}$
1991 [26]	Rotating parallel disk shear flow	Endothelial cells	Tissue culture plate	Max 3×10^4 cells attached after 7days
1993 [40]	Cone and plate rotational flow	Endothelial cells	Gelatin coated glass	Cell detachment begins at 40s of applied stress
1994 [27]	Shear flow by rotating plate	Endothelial cells	Fibronectin coated PC	Visual observation of cells. No measurements
1997 [23]	Shear flow by centrifugal force	HT1080 human fibrosarcoma	HIV-1 coated glass	~10% cell attachment, independent of shear flow
1997 [28]	Impulse shear flow in rotating parallel disks	Neurons	Glass	0.53 cell strain at $800 \text{ dynes}/_{\text{cm}}^2$ shear stress
1997 [9]	Shear flow by rotating plate	Rat osteosarcoma cells	Fibronectin coated glass	% remnant cells on surface
1998 [36]	Shear flow in channel	3T3 fibroblasts	Glass	0% cell attachment at 0.0068 dynes
2001 [33]	Jet impingement (impulse)	3T3 & L929 fibroblasts	Termanox, Stainless steel,	Max 3T3= $1060 \text{ dynes}/_{\text{cm}}^2$ in thermanox Max 929= $1060 \text{ dynes}/_{\text{cm}}^2$ on Stainless steel
2004 [22]	Shear flow in channel	WT NR6 fibroblast	Fibronectin coated glass	Minimum 5% cell adhesion after 12 min at $4000 \text{ dynes}/_{\text{cm}}^2$
2004 [7]	Shear flow in channel	Rat epitenon fibroblasts	PMMA	Flat surface ~190 cells Rough surface ~ 100 cells attached

CHAPTER II

MOTIVATION AND OBJECTIVES

As discussed in the Chapter I, incorporation of implants by the host is an important aspect in their success. Poor biocompatibility may develop into serious health complications. A study conducted in 1994 by Hakim et al. reported up to 75% mortality rate in patients with renal failure caused by poor biocompatibility of the material used for dialysis [41]. A study by Lang and Schiffel in 2000 showed a 21% improvement in the biocompatibility of dialyzer materials with a 54% mortality rate due to biocompatibility failure [42]. In 2008, Alonso et al. reported no significant difference in biocompatibility failure between patients with a biocompatible and non-biocompatible dialysis materials [43] even though biomaterials must undergo a rigorous cytotoxicity assessment prior to their use in patients. This biomaterial application had some improvements over the last years but failure due to poor biocompatibility is still an issue that should be addressed. Therefore, in vitro assessment of biocompatibility is a critical step.

The long term objective of this research is to understand and improve biocompatibility of materials. The first aim of this thesis research is to develop a methodology to assess the cell-material adhesion quantitatively. The second aim is to obtain fundamental understanding of cell-material adhesion mechanisms. Until now, all proposed systems to measure the adhesion between cell network and substrate have only been used for few cell types and a narrow material selection. For this reason, it is impractical and impossible to compare the level of biocompatibility of each material. Experimental approach will be used to accomplish the research goals. A parallel disk

rotating system will be employed because it has been extensively used to study biological systems and qualitatively understand the effect of substrate chemistry, surface roughness, and surface coatings on cell adhesion. The system, however, has not been used to quantitatively measure the cell adhesion strength to external surfaces.

Cells will be cultured on various surfaces and secured to the fixed disk of the test system. The shear stress generated by the system varies with radial position and is highest at the outer diameter and it decreases with decreasing radius. The maximum applied shear stress (τ_a) will be selected such that it exceeds the adhesion strength between the cells and the substrate. If the applied shear stress exceeds the cell-substrate adhesion strength, the cells will detach from the surface. Because the shear stress decreases with decreasing radius, it is expected that the shear stress will reach a critical point along the radius where the shear stress will be equal to the cell-substrate adhesion strength leaving a well-defined radius of cells on the surface. Any cells inside this critical point will remain unaffected because the shear stress experienced by them is lower than their adhesion strength.

The radius of cells left on the surface after testing is called the critical radius (R_C) and the shear stress experienced by the cells at this point is called the critical shear stress (τ_C). Figure 11 illustrates the expected results, a well defined R_C . The black arrow indicates the shear flow generated by the rotating disk.

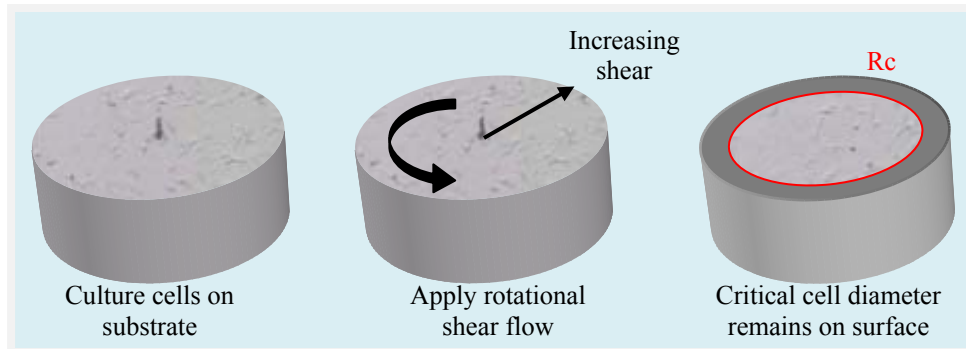


Figure 11 Test objectives. Cells are cultured on substrate and tested with parallel rotating disk to generate a shear flow.

It is expected that the proposed method will allow accurately measuring the adhesion strength at the cell-material interface. Analysis of the flow properties could provide significant and reliable information about the cell adhesion mechanisms. The significance for this research lies in the area of artificial implants and could allow considerable improvement in their design and lifetime.

CHAPTER III

EXPERIMENTS

This chapter discusses materials, equipments, and procedures for the research. Basic information of cells is provided.

3.1. Materials

3.1.1. Cell culture

3.1.1.1. Cells

As discussed in Chapter I, fibroblasts and neurons are two common cell types used for in-vitro studies. The fibroblasts and neurons are secondary and primary cultures respectively. A primary culture is one that is used after extracting and dissociating. A secondary culture is obtained after the first passage. Primary culture cells multiply over time and must be separated into at least 2 cultures. This separation process is called a passage and it is necessary to control cell growth and ensure all cells obtain the required nutrients from the cell culture media.

The NIH 3T3 Swiss mouse fibroblast cell culture used in this study was purchased as a primary culture from ATCC. This cell line is obtained from 13 to 16 day old Swiss mouse embryos as extracted by Todaro and Green in 1963. This cell line is widely used because cells maintain their structure and activity over extended periods of time and over many passages [44]. The 3T3 stands for 3-day transfer with a cell density of 3×10^5 cells for a 20cm^2 culture dish [44]. This cell line must be maintained at 37°C with a controlled 5% CO_2 environment and a pH of 7.4 [44-46]. The 3T3 fibroblasts

have an average cell diameter of $40\mu\text{m}$ and a $1\mu\text{m}$ cell height. The 3T3 fibroblasts used in this research are a secondary culture at their 12th to 15th passage. Figure 12 shows an attached fibroblast and lists the main components of these cells. Figure 13 shows an NIH 3T3 fibroblast cell culture.

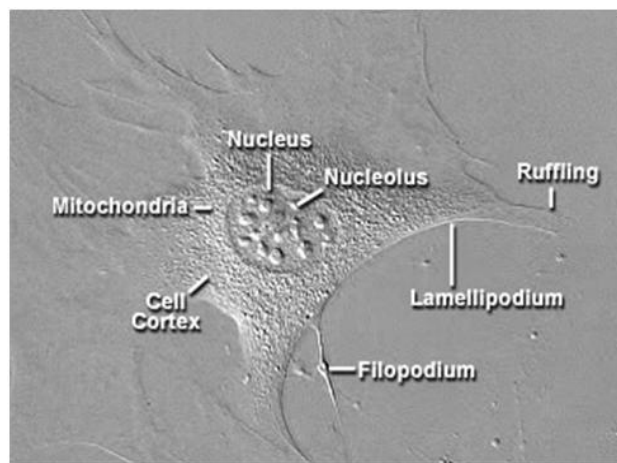


Figure 12 3T3 Swiss mouse fibroblast originally extracted by Todaro and Green. Image by Nikon MicroscopyU [47].



Figure 13 3T3 mouse fibroblasts at 3 days of culture on 2, 6 Bis(3 amino phenoxybenzo nitrile) (β -CN APB) at 10X magnification with an Axiovert A200 inverted transmission microscope (Carl Zeiss).

The neurons used in this work are bipolar neurons which are found in sensory systems like the eye, nose, and ear. The main characteristic of bipolar neuron cells is their shape; they have the body cell and one axon. The axon is a fiber that transfers information to other cells or to other parts of the nervous system. The extraction procedure was first implemented by Moscona in 1960 [48]. This cells are widely used for neuron communication analysis because they allow easy comparison of in-vivo and in-vitro results [49]. The cell culture was directly extracted from 6-day chick embryos obtained from the Poultry Science Department at Texas A&M University in College Station, TX. This cell line must be maintained at 39°C with a controlled 5% CO₂ environment and pH of 8.2 [13]. Chick retina neuron cells are approximately 10µm diameter.

Figure 14 shows a diagram of a bipolar neuron and three bipolar neurons extracted from the retina of a 6day chick embryo. Figure 15 shows a bulk cell culture of the 6 day chick embryo neurons after 24 hours of cell seeding.

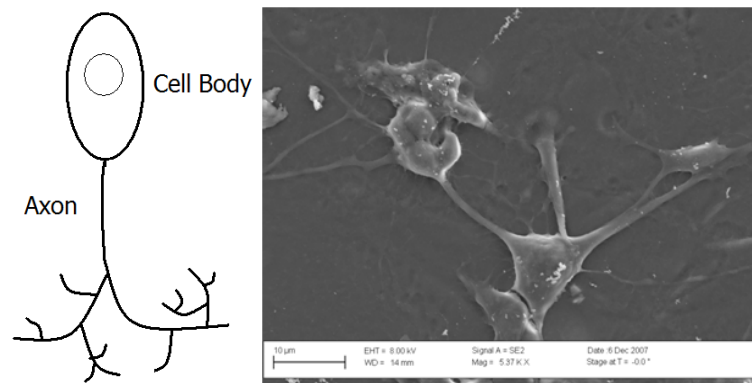


Figure 14 Bipolar neurons extracted from the retina of 6day chick embryos taken after 5 days of culture. Courtesy of Dr. Subrata Kundu.

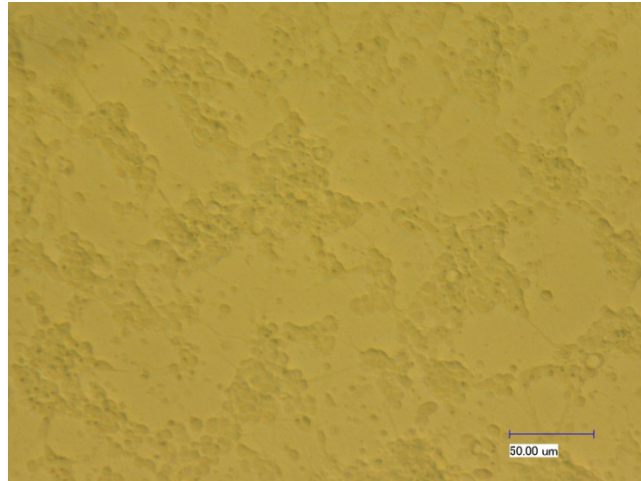


Figure 15 Bipolar neuron cells from 6-day chick retina cultured on PDL coated glass with 1000X under a VHX-600 3D digital microscope (Keyence Microscope).

3.1.1.2. Cell preparation and activation

Fibroblast cell cultures are pelletized and stored at cryogenic temperatures to allow shipping and storage for extended periods of time. The cells must be re-activated prior to use. Re-activation is a thermal and chemical process. Trypsin is used in NIH 3T3 mouse fibroblast cultures to re-suspend the cells and was purchased from Cell Applications, Inc. Trypsin can be extracted from the pancreas of animals and it is easily purified. It must be stored at -20°C [11].

The chick retina neurons are a primary culture and do not require storage. However, the extracted retina tissue must be dissociated prior to seeding. Culture dissociation is an electrochemical process. The retina is dissociated in a mixture of a saline solution and trypsin and are minced manually [50].

3.1.1.3. Culture media

Cell cultures are vulnerable to bacteria in the environment because they are not protected by the ECM, which also provides nutrients to the cells. For this reason, cell cultures must be maintained under a controlled media that provides the nutrients and protection against bacteria. The media used for the 3T3 fibroblast culture was Dubelcco's modified Eagle's medium and the media used for the chick neuron culture was Eagle's medium. Eagle's medium is made of L-amino acids, vitamins, salts, glucose, serum and antibiotics. Dubelcco's modification to Eagle's medium consists of adding 6-parts horse serum and 3 parts chick embryo extract to 8 parts Eagle's medium [51]. Table 3 lists all the components used to prepare Eagle's medium. The antibiotics used and the serum vary with cell culture to allow optimal results.

Table 3 Components of Eagle's medium.

L-Amino acids		Vitamins		Miscellaneous	
	mg/L		mg/L		%
Arginine	17.4	Biotin	10^{-6}	Glucose	0.1
Cystine	9.6	Choline	10^{-6}	Human serum	5.0
Glutamine	292.0	Folic acid	10^{-6}	Penicillin	0.005
Histidine	6.2	Nicotinamide	10^{-6}	Streptomycin	0.005
Isoleucine	26.0	Pantothenic acid	10^{-6}	Phenol red	0.0005
Leucine	20.0	Pyridoxal	10^{-6}	Salts	
Lysine	22.0	Thiamine	10^{-6}		%
Methionine	7.4	Riboflavin	10^{-7}	NaCl	0.68
Phenlalanine	13.2			KCl	0.04
Threonine	18.0			NaH ₂ PO ₄ •H ₂ O	0.014
Tryptophan	3.0			NaHCO ₃	0.22
Tyrosine	18.1			CaCl ₂	0.02
Valine	17.5			MgCl ₂	0.008

The serum and antibiotics used depends on the cell culture. NIH 3T3 mouse fibroblasts medium was supplemented with 10% bovine calf serum and

penicillin/streptomycin. The Dubelco's modified Eagle's medium was purchased from Cell Applications, Inc. Chick retina neurons are maintained under Eagle's medium, enhanced with 10% heat-inactivated horse serum, both from BioWhittaker, with 2 mMol glutamine, 50 U/ml penicillin, 50 g/ml streptomycin, and 20 ng/ml recombinant rat ciliary neurotrophic factor all from R&D Systems [49, 50].

3.1.1.4. Substrates for cell culture

Polymers, metals, semiconductors, and ceramic materials were selected as substrates for cell culture. Most of the materials selected are already being used or have the potential of being used as biomaterials as summarized in Table 4.

Table 4 Materials used as substrates for cell culture experiments.

Substrate Material	Biocompatible	Application	Ref
PMMA	Yes	Dental cement	[12]
UHMWPE	Yes	Artificial joints	[52]
PC	Yes	Renal dialysis material Surgical instruments	[43]
Epoxy	Yes	Dental sealer	[53]
PVDF	Yes	Suture	[54]
NiCu coated PVDF	Not tested	Potential for cell electrical characterization	
Ag coated PVDF	Silver – no	Potential for cell electrical characterization	[55]
Au coated PVDF	Gold – yes	Potential for cell electrical characterization	
Si Wafer	No	Potential for cell electrical characterization	
RS 100	Not tested	Ceramic material, potential for implants	
Glass	Yes	Cell culture dishware	

Some materials were selected to test the possibility for use in cell characterization; to measure elastic, chemical, and electrical properties of the cell. Glass

substrates were only used for the chick neuron cultures and all other materials were used in the fibroblast cultures. The glass substrates are microscope slides purchased from Fisher Scientific. The substrates were coated with poly-D-lysine purchased from Sigma Aldrich.

3.1.1.5. **Cell culture dishware**

The 3T3 fibroblasts were cultured for passage in a T75 (75cm² surface area) flask. The fibroblast cultured samples were prepared and maintained in a 6-well culture plate (Falcon). The wells have a diameter of 34.8mm each. The chick retina neuron cells were cultured in 25mm diameter glass microscope slides. The cultures were maintained in individual Petri dishes of 50mm diameter.

3.1.2. **Materials for testing**

The fluid used to generate the rotating flow was a phosphate buffered saline solution (PBS) purchased from Sigma-Aldrich. PBS contains NaCl, KCl, Na₂HPO₄, KH₂PO₄, CaCl₂, MgCl₂•6H₂O in distilled water [51]. There are some slight variations in the quantities used depending on the cell culture it is used for. A high strength double-sided tape is used to secure the sample to the fixed disk. The tape is selected with adhesive strength of at least one order of magnitude higher than the expected adhesion strength between cells and substrates.

3.1.3. **Cell fixatives**

Fibroblast cultures were stained with Calcein AM from BD™ Fluorescent Dyes prior to testing. The tested cell samples were fixed in formalin for 24 hours and

dehydrated with increasing concentrations of ethanol. Chick neuron cultures were fixed with Zamboni's fixation from Newcomer Supply.

3.2. Equipment

3.2.1. Imaging equipment

Optical microscopes are used to analyze cell cultures before and after testing. Imaging before testing is essential to determine the quality of cell culture. Imaging after testing is required to observe if the critical diameter of cells was left on the surface.

An Axiovert 200 inverted transmission microscope with fluorescent light source was used to observe 3T3 fibroblast cultures before and after testing. The 3T3 fibroblast culture samples were also imaged using a JEOL JSM-6400 Scanning Electron Microscope (SEM) after testing, fixing and dehydrating. The chick retina cell cultures were imaged before and after testing with VHX-600 3D digital image microscope from Keyence. Figures 16, 17, and 18 show the Axiovert 200, the Keyence VHX-600 microscope and the JEOL JSM-6400 SEM respectively.



Figure 16 Carl Zeiss inverted transmission microscope (Axiovert 200).
Image from Carl Zeiss [56].



Figure 17 VHX-600 3D microscope from Keyence.

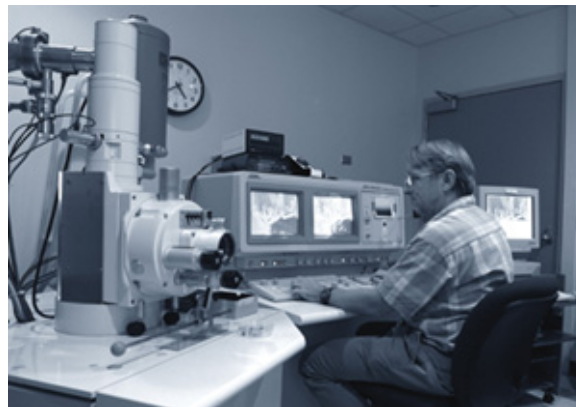


Figure 18 JEOL JSM-6400 Scanning Electron Microscope in the Microscopy & Imaging Center at Texas A&M University [57].

3.2.2. Cell culture equipment

Cell cultures are handled inside a laminar flow fume hood equipped with a UV light. This helps maintain the cultures free of bacteria. The cell cultures are maintained in an incubator with controlled temperature and % CO₂ environment. The fibroblasts are maintained at 37°C and the chick neurons are maintained at 39°C. Other equipment necessary for cell culture are a centrifuge, and a hemacytometer. The centrifuge is used to pelletize the cells prior to dispersion and the hemacytometer is a microscope slide

with a standard size grid to help count the number of cells/volume. Figure 19 shows an incubator used to control temperature and %CO₂ environment for cells.



Figure 19 Cell culture incubator from Lab Line.

3.2.3. Surface measuring equipment

The surface roughness of all the samples was measured with a TR200 Profilometer from Qualitest, shown in Figure 20. The stylus moves in a straight line for 0.5 in. It measures the average pore size and calculates the average surface roughness (Ra). The Ra is the average of the peaks and valleys over the measured distance.



Figure 20 TR200 Profilometer from Qualitest.

3.2.4. Rheometer

A rheometer is used to measure the flow properties of liquids. Rheometers are capable of measuring stress and deformation of a liquid [58]. An AR-G2 Rheometer with parallel disk geometry from TA Instruments was used for this research. The basic components in a rheometer are the motor, spindle (rotating disk), and a fixed disk. The motor is torque driven and allows for easy control of rotational velocity, and oscillation frequency. Figure 21 illustrates the basic components of a parallel disk rotational rheometer. Figure 22 is the AR-G2 parallel disk rheometer from TA Instruments used in this work.

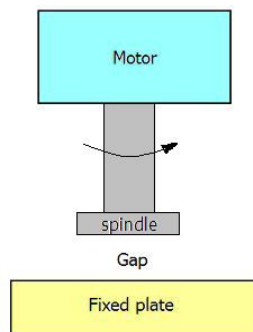


Figure 21 Diagram of parallel plate rotational rheometer with basic components.

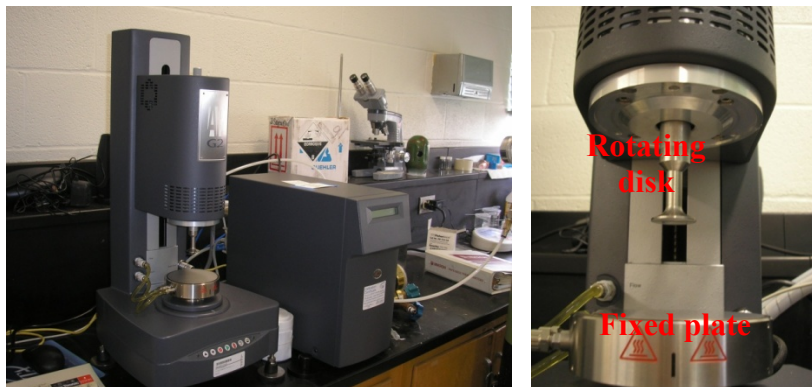


Figure 22 AR-G2 Rheometer from TA Instruments.

The parallel plate rotational rheometer was selected for this research because it applies a controlled shear stress throughout the test. The instrument is torque driven, however, any parameter can be controlled through a feed-back loop that adjusts the motor's torque. The instrument controls the temperature of the sample during testing, which is essential when working with live cell cultures. It measures the rotational velocity, torque, and viscosity of the media and allows to accurately control the distance between plates during the test. These parameters are necessary to the analysis of the rotational flow. The rheometer has been extensively used to study the factors affecting blood flow and some other properties of biofluids [59].

3.2.5. Surface cleaning and cell storage

Other miscellaneous equipment includes a short wave UV light, Autoclave, refrigerators and freezers. The UV light is used to maintain working surfaces in the laminar fume hood and culture materials free of bacteria. An autoclave is used to sterilize any instruments used during cell culture like tweezers and culture dishes. Refrigerators and freezers are required to store trypsin and cell culture media.

3.3. Methods

3.3.1. Cell cultures

3.3.1.1. Solutions for fibroblast culture

PBS prepared by mixing

- a. Mix then autoclave 8.0g NaCl, 0.2g KCl, 1.15g Na₂HPO₄, and 800 mL of distilled water.

- b. Mix then autoclave 0.1g CaCl_2 in 100mL of distilled water.
- c. Mix then autoclave 0.1g $\text{MgCl}_2 \cdot 6\text{H}_2\text{O}$ in 100mL of water.
- d. Mix a, b, and c, solutions after autoclaved and cooled.
- e. Add distilled water to complete 1L of solution.

Dissociating solution, used to separate tissues into cells

- a. Heat the PBS and trypsin separately to 37°C.
- b. Mix PBS and 0.25% trypsin and syringe repeatedly to mix the solution.

Cell culture media

- a. Made by mixing all ingredients listed in Table 3. With 10% bovine calf serum and penicillin/streptomycin.

3.3.1.2. Fibroblast culture substrates

- a. All materials used for culture substrates were cut in $3 \times 3 \text{cm}^2$ squares with thickness as received.
- b. The substrates were cleaned by rinsing in alcohol, allowed to air dry, and placing under shortwave UV light in laminar flow fume hood for 24 hours prior to cell seeding.
- c. The substrates were placed in a 6-well plate (Falcon). One substrate per well.
- d. A sterilized UHMWPE ring with 2.5cm internal diameter was used to hold samples down and avoid sample flotation.

3.3.1.3. Fibroblast culture

Original or primary cells are those obtained directly from 16-day Swiss mouse embryos. Transfer or secondary cells are those obtained by cell mitosis from pre-cultured cells.

Primary cell culture [44]

- a. Pulverize the Swiss mouse embryo.
- b. Mix with dissociating solution (PBS and trypsin). Wait 10 to 15 minutes to allow trypsin to separate the cells.
- c. Centrifuge the mixture. The cells will pelletize at the bottom of the test tube. Remove all the mixture.
- d. Rinse with PBS 3 times. Use twice as much PBS per rinse than trypsin used to stop the trypsin reaction.
- e. Add 10mL of culture media and pipette vigorously to dissociate the pellet and allow cells to float in media.
- f. Pipette 0.1 μ L of the suspended cells to count the #cells/volume with a hemacytometer. Repeat this step two or three times to verify cell dispersion.
- g. Add media to achieve the desired #cells/volume in the solution.
- h. Cells are placed in T75 culture flask or similar container.
 - o Cells can also be placed directly on substrate materials if a primary culture is required for testing.
- i. Maintain the cultured cells in incubator with 5% CO₂ environment at 37°C.

Secondary cultures are obtained from passage of primary cultures after 3 days of original culture the number of cells in the culture multiply threefold in approximately 3 days. Therefore, the culture from one flask can be transferred into 3 every 3 days.

Seeding cells onto substrate materials

- a. From the T75 cell culture flask with cells, remove cell culture media.
Perform this step carefully to not disturb the cells, which are attached at the bottom of the flask.
- b. Prepare the dissociating solution (PBS and trypsin at 37°C).
- c. Pipette approximately 3mL of solution to the flask to detach cells from the flask wall. Pipette several times to ensure all surface has been covered.
- d. Wait 10 to 15 minutes until all cells seem mobile (detached).
- e. Pipette cells in dissociating solution from container and centrifuge to pelletize the cells. Remove all dissociating solution.
- f. Rinse with PBS 3 times. Use twice as much PBS per rinse than trypsin used to stop the trypsin reaction.
- g. Add 10mL of culture media and pipette vigorously to dissociate the pellet and allow cells to float in media.
- h. Pipette 0.1 μ L of the suspended cells to count the #cells/volume with a hemacytometer. Repeat this step two or three times to verify cell dispersion.
- i. Add media to achieve the desired #cells/volume in the solution.
- j. Seed 5,000 cells/cm² over each substrate and place in incubator with 5% CO₂ environment at 37°C.

- k. Allow 24 hours prior to testing to allow cells to attach to the substrate.

3.3.1.4. **Prepare fibroblast samples for imaging**

Samples are dyed with Calcein AM prior to testing to allow fluorescent imaging and are fixed in formalin for 24 hours after testing. The samples cell seeded substrates are dehydrated in increasing concentration of ethanol, starting from 75% to 100% and allowed to air dry. The samples are then coated with palladium for SEM imaging.

3.3.1.5. **Solutions for neuron culture**

PBS for chick neuron culture is prepared by mixing then autoclaving 123mMol NaCl, 5.36mMol KCl, 9.51mMol Na₂HPO₄, 1.48mMol NaH₂PO₄, 0.1 gm/ml glucose in 1L of distilled water. The dissociating solution is prepared the same as for the 3T3 fibroblast culture with 05mg/mL of trypsin. The cell culture media is made by mixing all ingredients listed in Table 3 with 10% heat-inactivated horse serum, 2 mMol glutamine, 50 U/ml penicillin, 50 g/ml streptomycin, and 20 ng/ml recombinant rat ciliary neurotrophic factor.

3.3.1.6. **Neuron culture substrates**

The glass substrates must be cleaned and coated with PDL prior to cell seeding. Glass microscope slides with 25mm diameter are used for substrates in the chick embryo neuron culture.

- a. Clean glass microscope slides in HNO₃ for 2 days.
- b. Rinse substrate in water for 6 hours and dry individually.
- c. Prepare a mixture of borate buffer: 0.682g boric acid, 0.858 g sodium tetraborate, add to 100 ml distilled water, and adjust the pH to 8.4.

- d. Add 1 mg/mL of poly-D-lysine and stir for 15 minutes.
- e. Place 5 to 10 substrates in a 35mm Petri dish and fill with 5mL of borate buffer and poly-D-lysine mixture. Make sure substrates do not overlap.
- f. Let sit in mixture for at least 1 to 2 hours.
- g. Rinse 7 times with distilled water and let sit in distilled water for 1 hour.
- h. Place substrates in individual 35mm Petri dishes.
- i. Leave in laminar fume hood under UV light overnight.
- j. Close each Petri dish and store in refrigerator for up to 3 weeks.

3.3.1.7. **Neuron culture**

For the case of chick retina neuron cells, only primary cultures are used [50].

- a. Incubate the fertilized eggs for at 39°C for 6 days.
- b. Remove chick from egg and sacrifice the chick.
- c. Remove and open the eye to extract the retina.
- d. The retina is placed in dissociating solution of PBS and trypsin for 25 minutes and pulverized with a pipette.
- e. Centrifuge the mixture. The cells will pelletize at the bottom of the test tube. Remove all the mixture.
- f. Rinse with PBS 3 times. Use twice as much PBS per rinse than trypsin used to stop the trypsin reaction.
- g. Add 10mL of culture media and pipette vigorously to dissociate the pellet and allow cells to float in media.

- h. Pipette 0.1 μ L of the suspended cells to count the number of cells per volume with a hemacytometer. Repeat this step two or three times to verify cell dispersion.
- i. Add media to achieve the desired number of cells per volume in the solution.
- j. Calculate the required cell number to cover approximately 70% of the substrate surface.
- k. Place neuron seeded substrates in incubator with 5% CO₂ environment at 39°C.
- l. Allow 24 hours prior to testing to allow cells to attach to the substrate.

3.3.1.8. **Prepare neuron samples for imaging**

Samples are placed for 10 minutes in Zamboni's fixation after testing and are then rinsed 3 times with PBS for five minutes each and allowed to air dry.

3.3.2. **Testing conditions**

The cell cultured substrate is secured to the lower fixed disk. The rotating disk is lowered to a controlled distance from the lower plate. The gap is filled with PBS. The upper plate rotates generating a shear flow with the PBS on the cells. The diameter of the rotating disk is 25mm. The sample is secured on the lower fixed disk with high strength double sided tape. The adhesion strength of the tape was selected such that it would be one or two orders of magnitude higher than the expected adhesion strength of cells to the selected substrates. Figure 23 shows a schematic of the test set up.

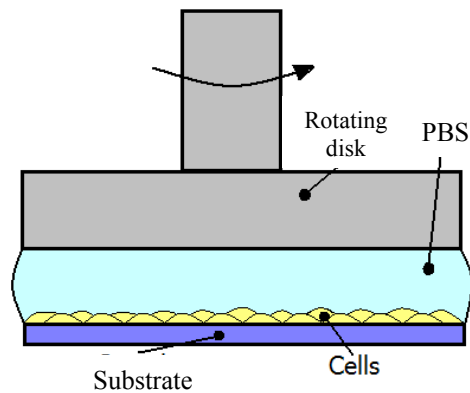


Figure 23 Experimental set up. The cell cultured substrate is secured to the lower disk.

The cell adhesion test procedure consists of applying a constant maximum rotational shear stress (τ_a), which is maximum along the outside diameter. The sample was inspected after testing to verify the presence of a critical radius of cells left on the surface (R_C). The R_C is measured and used in a rotational flow analysis to calculate the critical shear stress (τ_C) of bulk cell adhesion to the substrate.

A creep test procedure was used in this work. This test procedure applies a controlled maximum shear stress and measures the sample deformation as a shear strain. The temperature and distance between rotating and fixed disk is controlled during testing. The test has a duration of 10 minutes, this time is selected to guarantee the flow conditions have reached equilibrium. The AR-G2 Rheometer measures the viscosity, angular velocity, and shear strain among many other parameters. Once the test is complete, the cell seeded sample is fixed and imaged accordingly.

CHAPTER IV

RESULTS

The objective of this research is to develop a methodology to evaluate cell adhesion strength quantitatively. A parallel disk system is used here to study the adhesion mechanisms of fibroblast cells. The fluid shear is analyzed for the cells cultured on various materials having different surface properties. This chapter presents the most relevant and significant results obtained for the proposed method.

4.1. NIH 3T3 Swiss mouse fibroblasts

The adhesion of NIH 3T3 Swiss mouse fibroblasts to several substrates was measured to determine if the system could be used to distinguish the adhesion between materials. The τ_a is the maximum controlled shear stress applied. These values are selected for shear testing based on values reported in the literature for polymeric materials. The values of τ_a varied from 5 to 45 dynes/cm². Table 5 lists all tests performed; the numbers in parenthesis specify the number of tests repeated at the given τ_a . For example, the PMMA 35 (4X) indicates that 4 PMMA samples were tested at 35 dynes/cm². The testing conditions were 480 μ m gap for 10 min with 37°C temperature for all samples.

Table 5 Test conditions for NIH 3T3 Swiss mouse fibroblasts.

Substrate	τ_a (dyne/cm^2)
PMMA	35 (4X), 20 (2X), 25 (3X)
UHMWPE	35, 25, 20, 15 (2X), 5 (2X)
PC	25 (2X), 15, 20 (2X), 10
Epoxy	20, 35 (3X), 25 (3X), 30, 40, 45
PVDF	35, 15
NiCu coated PVDF	35, 15 (2X), 25
Ag coated PVDF	No cell adhesion
Au coated PVDF	30 (2X), 20
Si Wafer	No cell adhesion
RS 100	25, 15(2X), 5

A total of 47 tests were completed on NIH 3T3 Swiss mouse fibroblasts. There are three factors found to affect the cell adhesion, such as staining solution, substrate materials, and SEM preparation. In addition, 7 samples were discarded due to low cell density because the cells on these samples attached to the Petri dish instead of the substrate. Sample damage can be separated into damage before testing and damage after testing. Table 6 shows 27 samples damaged before testing.

Table 6 NIH 3T3 Swiss mouse fibroblasts samples damaged before testing.

Sample	τ_{applied} ($\frac{\text{dyne}}{\text{cm}^2}$)	Observations
Epoxy_25_01	25	~80% cell death – high staining concentration
Epoxy_25_02	25	Ibid
Epoxy_35_01	30	Ibid
NiCu/PVDF_35_01	35	Ibid
PC_25_01	25	Ibid
PMMA_20_01	20	Ibid
PMMA_25_01	25	Ibid
PMMA_25_02	25	Ibid
PMMA_35_01	35	Ibid
PMMA_35_02	35	Ibid
PVDF_35_01	35	Ibid
RS-100_25_01	25	Ibid
UHMWPE_20_01	20	Ibid
UHMWPE_25_01	25	Ibid
UHMWPE-35_01	35	Ibid
NiCu/PVDF_15_02	15	Cells not attached
NiCu/PVDF_25_01	25	Ibid
NiCu/PVDF_15_01	15	Ibid
Si wafer_15_01	15	Ibid
Si wafer_25_01	25	Ibid
Epoxy_20_01	20	Low cell density. The cells collected at bottom
PC_15_01	15	Ibid
PMMA_20_02	20	Ibid
PMMA_35_03	35	Ibid
PVDF_15_01	15	Ibid
UHMWPE_15_01	15	Ibid
UHMWPE_5_01	5	Ibid

One of the damages was due to excess concentration of the staining solution applied before testing which caused death on more than 80% of the cell culture. Five samples showed that cell adhesion strength to the nickel copper (NiCu) coated PVDF and the silicon (Si) wafer samples was weak. The cells on these samples detached during sample transfer. Seven samples had very low cell density which made it difficult to

measure the cell adhesion. The remaining 20 samples showed an R_c after testing. Since some samples were opaque, they could not be imaged with the Axiovert transmission microscope. Therefore, the samples were prepared for SEM imaging. The samples were fixed and dehydrated after testing for SEM imaging. Some of the chemicals used for these steps damaged the surface of 17 samples and the R_c could not be measured as listed in Table 7. Testing conditions were 480 μ m gap for 10 min with 37°C temperature.

Table 7 3T3 Swiss mouse fibroblasts samples damaged after testing.

Sample	τ applied (dyne/cm ²)	Observations
Epoxy_25_03	25	R_c observed. Damaged during SEM preparation
Epoxy_30_01	30	ibid
Epoxy_40_01	40	ibid
Au/PVDF_30_01	30	ibid
Au/PVDF_30_02	30	ibid
Epoxy_45_01	45	ibid
PC_20_01	20	ibid
PC_25_02	25	ibid
PMMA_35_04	35	ibid
PC_20_02	20	ibid
Epoxy_35_03	35	ibid
Epoxy_35_02	35	ibid
RS100_05_01	5	Opaque sample. Cannot see cells in SEM
RS100_15_01	15	ibid
RS100_15_02	15	ibid
UHMWPE_05_02	5	ibid
UHMWPE_15_02	15	ibid

The samples that allowed for cell adhesion measurements are listed in Table 8. Here the samples are named as follows: substrate, applied shear stress in dynes/cm² and the test number. The critical radius (R_c) measured after testing is also listed in the table.

Table 8 The NIH 3T3 Swiss mouse fibroblasts shear strength adhesion.

Sample	τ_a (dyne/cm ²)	R _C (cm)
PMMA_25_03	25	1.05 ±0.015
Au/PVDF_20_01	20	0.70 ±0.025
PC_10_01	10	0.636 ±0.008

Figures 24 to 26 show the well-defined R_C for the NIH 3T3 Swiss mouse fibroblasts tested on various substrates. Figure 24a-f show the R_C of PMMA_25_03 and Figure 24g illustrates the imaging points. Figure 25 shows the R_C of Au/PVDF_20_01 and. Figure 26a-f show the R_C of PC_10_01 and Figure 26g illustrates the imaging points. All samples show cell detachment along a well-defined critical diameter.

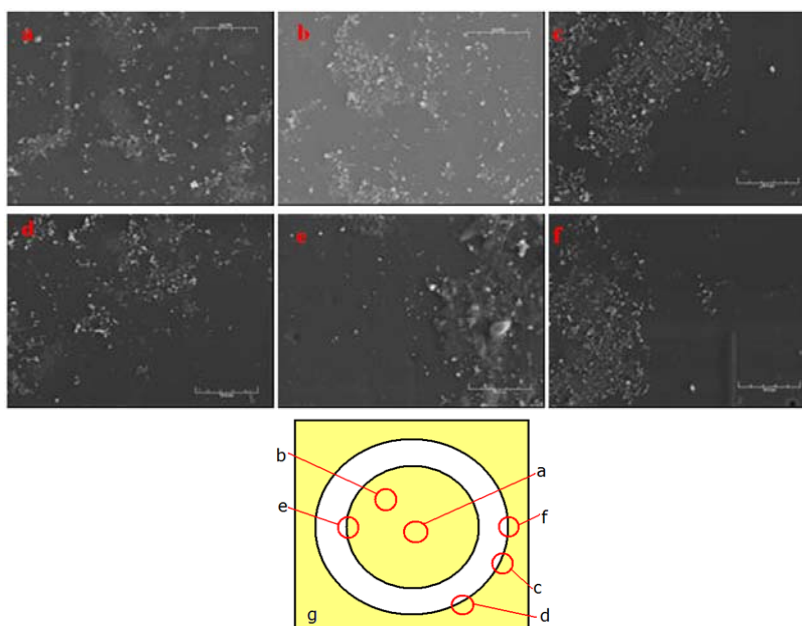


Figure 24 SEM images of Ra = 0.636cm of PMMA_25_03. The imaging points are shown in 2g. The line scale is equivalent to 30 μ m.

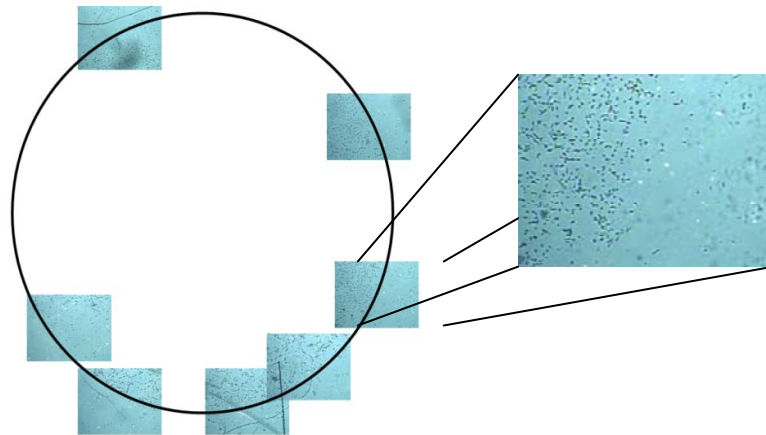


Figure 25 $R_c = 0.70$ cm for Au/PVDF_20_01. Image obtained with Axiovert inverted transmission microscope.

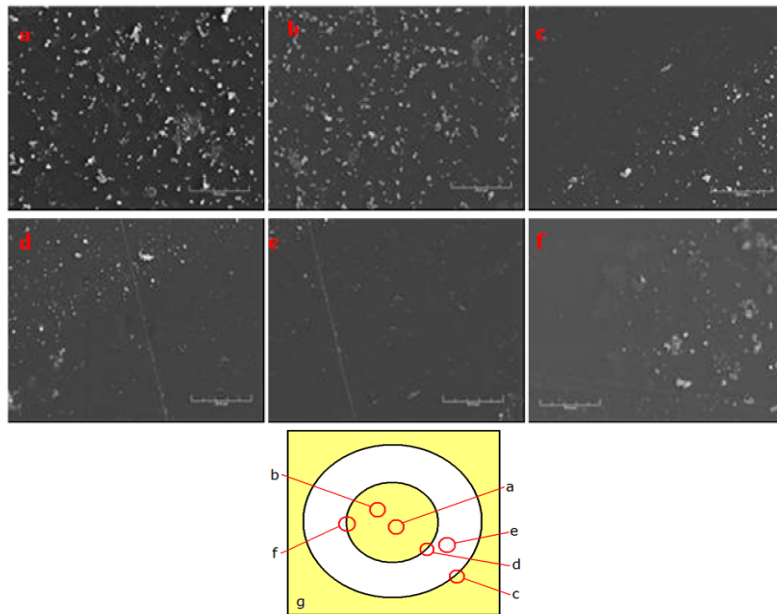


Figure 26 SEM images of $R_a = 1.05$ cm for PC_10_01. The imaging points are shown in 2g. The line scale is equivalent to $30 \mu\text{m}$.

4.2. Chick embryo retina neurons

A total of 25 chick embryo neuron cell samples were tested. The substrate used was poly-D-lysine coated glass. The samples were simply numbered in increments of one along with the applied shear stress in dynes/cm^2 . An example is S15_10; this

indicates that it was sample (S) number 15 in the series with $\tau_a=10$ dyne/cm². Table 9 lists all samples and test conditions used for chick neurons on PDL coated glass samples.

Table 9 Test conditions for chick embryo neuron cells.

Sample	τ_a (dyne/cm ²)	Gap (μ m)	Time (min)	Temp (°C)	Observations
S01_10	10	950	10	39	Poor cell dispersion
S02_10	10	950	10	39	Ibid
S03_05	5	780	10	39	Ibid
S04_15	15	780	10	39	Ibid
S05_10	10	780	10	39	Ibid
S06_10	10	500	10	39	Sample broke after test
S07_	-	-	-	-	Sample broke before test
S08_	-	-	-	-	Ibid
S09_10	10	800	10	39	Poor cell dispersion
S10_10	10	1000	10	39	Ibid
S11_10	10	1500	10	39	Ibid
S12_05	5	500	10	39	Ibid
S13_30	30	500	10	39	Ibid
S14_25	25	500	10	39	Ibid
S15_10	10	500	10	39	Test OK. Well-defined Rc
S16_25	25	500	10	39	Ibid
S17_40	40	500	10	39	Ibid
S18_55	55	500	10	39	Sample broke after tests
S19_55	55	500	10	39	Test OK. Well-defined Rc
S20_70	70	500	10	39	ibid
S21_10	10	700	10	39	Sample broke after test
S22_25	25	500	10	39	Ibid
S23_30	30	500	10	39	Ibid
S24_25	25	500	05	39	Test OK. Well-defined Rc
S25_30	30	500	05	39	Ibid

Glass is a control surface in cell culture studies. It is generally used as a substrate when cell behavior is analyzed. In this study, the glass substrate is used to verify the reliability of the proposed shear flow system. The τ_a ranged from 10 dynes/cm² up to 70 dynes/cm² in increments of 5 or 10 dynes/cm² for the samples tested. A total of 11

samples were discarded due to uneven cell dispersion and excessive cell agglomeration, and 7 samples broke before or after testing. Table 10 summarizes the results of chick neuron cells on PDL coated glass substrates. The samples are named as follows:

Sample#_ τ_a .

Table 10 Results of chick embryo neuron cells on poly-D-lysine coated glass substrates.

Sample	τ_{applied} (dyne/cm ²)	R _c (cm)
S15_10	10	1.158 ±0.004
S16_25	25	0.976 ±0.006
S17_40	40	0.663 ±0.020
S19_55	55	0.631 ±0.050
S20_70	70	0.483 ±0.075
S24_25	25	0.933 ±0.005
S25_30	30	0.394 ±0.005

Figures 27 through 33 show a well-defined R_c for the neuron cell cultures. The images of the R_c are presented in the same order as in Table 10.



Figure 27 R_c=1.158cm for S15_10. With VHX-600 Keyence microscope. The scale bar indicates 500 μ m.

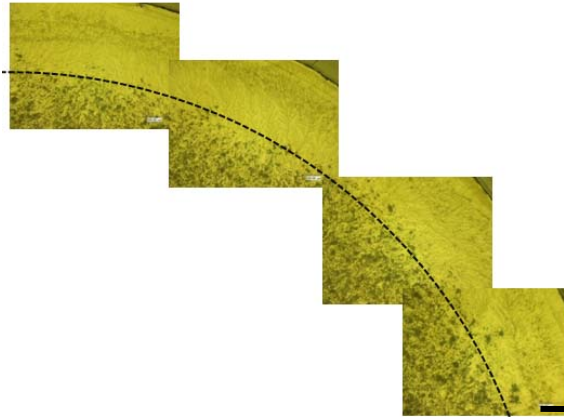


Figure 28 $R_c=0.976\text{cm}$ for S16_25. With VHX-600 Keyence microscope. The scale bar indicates $500\mu\text{m}$.

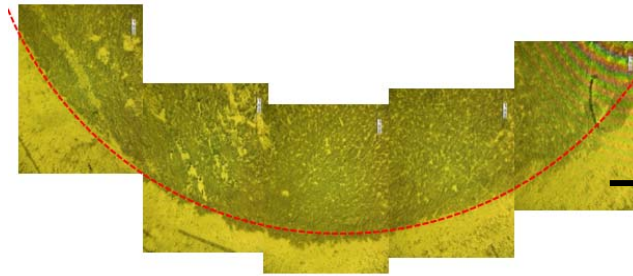


Figure 29 $R_c=0.663\text{cm}$ for S17_40. With VHX-600 Keyence microscope. The scale bar indicates $500\mu\text{m}$.



Figure 30 $R_c=0.631\text{cm}$ for S19_55. With VHX-600 Keyence microscope. The scale bar indicates $500\mu\text{m}$.

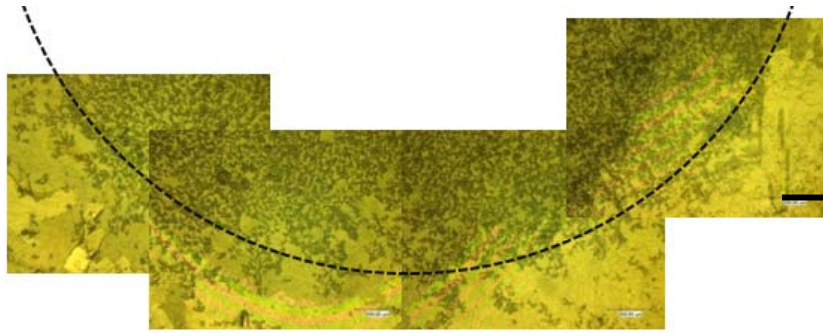


Figure 31 $R_c=0.483\text{cm}$ for S20_70. With VHX-600 Keyence microscope. The scale bar indicates $500\mu\text{m}$.

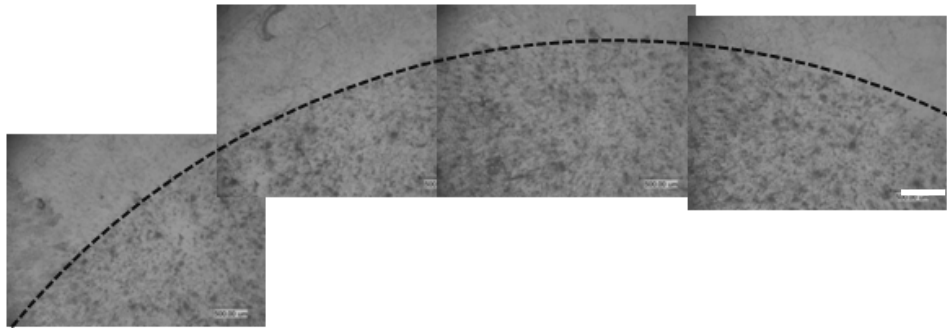


Figure 32 $R_c=0.933\text{cm}$ for S24_25. With VHX-600 Keyence microscope. The scale bar indicates $500\mu\text{m}$.

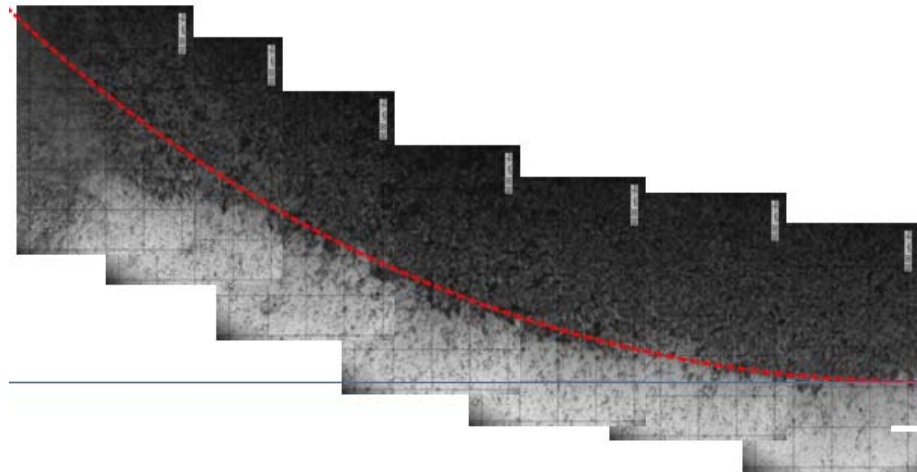


Figure 33 $R_c=0.394\text{cm}$ for S25_30. With VHX-600 Keyence microscope. The grid is $50\mu\text{m}/\text{div}$.

Variations in R_c are due to a “paperclip effect” where if one paperclip is pulled from a box, it is very likely that several will be entangled with it and come out too. If the cell density is too high (>70% surface coverage), the connections between cells will pull other cells that are still attached on the surface. This results in an uneven or rough R_c edge on some parts of the sample. However, it was the connections between cells that detached the other cells inside the R_c .

The R_c of remnant cells after testing is inversely proportional to the applied shear stress. As more shear stress is introduced to the cells, more cells detached leaving a smaller radius of cells on the surface. This trend can be observed in the critical radius vs. applied shear stress diagram shown in Figure 34. The values seem to converge to a radius of approximately 0.50cm. All values follow a smooth trend except for the critical radius measured for S25_30, which is highlighted with a circle. One likely reason for this test is that the scale bar, which is set manually for the Keyence microscope used, was not set correctly yielding a lower R_c when measured.

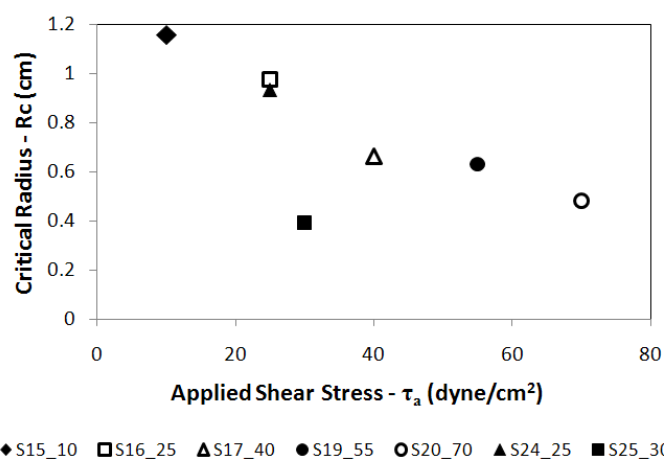


Figure 34 Results of chick neurons on PDL coated glass. The R_c is inversely proportional to τ_a .

The results demonstrate that the parallel disk system can be used to measure the cell adhesion strength. A well-defined critical radius of cells remains on the surface after testing. The critical radius is measured and used to calculate the adhesion strength of the cells, which ranged between 9.26 and 27.8 dynes/cm² depending on the applied shear stress.

The results obtained for the NIH 3T3 Swiss mouse fibroblasts on PMMA, PC, and gold coated PVDF demonstrate that the parallel disk rotational system can be used to quantitatively measure the cell adhesion strength of cells to various substrates. The experiments conducted on the chick embryo neurons adhered to poly-D-lysine coated glass are used to demonstrate the repeatability of the system and to further understand the interaction at the cell-substrate interface.

In general, the proposed methodology to measure and quantify the cell adhesion strength has shown to be effective for two different cell lines and on various substrates. Additionally, the chick embryo neuron samples S16_25 and S24_25, which were tested at 25 dynes/cm² shear stress, show critical radii of 0.976 and 0.933 cm respectively. There is a 4.41% difference between the measured critical radii between these two samples. This demonstrates that reproducible results can be obtained with this system.

CHAPTER V

MECHANISMS OF CELL ADHESION

Results in Chapter IV showed that the fluid shear of a rotational disk reflects the cell adhesion. In this chapter, analysis of fluid flow, elastic and adhesion properties of cells, and factors affecting cell adhesion are conducted.

5.1. Analysis of parallel disk rotational flow

Understanding the flow properties of the parallel disk geometry used in this study is necessary to analyze the critical shear stress, which indicates the adhesion strength of cells onto substrates. The flow properties of the rotating parallel disk have been extensively studied because it is a standard geometry of the rheometer and has been used in biological systems and well as in other fields as discussed in Chapter I.

The results obtained for the 3T3 fibroblasts on PMMA, PC, and Au/PVDF are summarized in Table 8 in the previous chapter. The well-defined radius of cells that remains after the test demonstrate that the adhesion shear stress can be calculated. The R_c for each sample is shown in Figures 24 to 26. The results demonstrate that the adhesion strength of fibroblasts is highest for PMMA followed by Au/PVDF and PC with an R_c of 1.05cm, 0.70cm, 0.636cm and respectively. The results of chick neurons on PDL coated glass are summarized in Table 10 and indicate that the R_c varies with applied stress. A shear stress ranging between 10dynes/cm² and 70 dynes/cm² was applied resulting in a measured R_c from 1.158 cm to 0.483 cm respectively. The R_c obtained for chick neurons on PDL coated glass are shown in Figures 27 to 33. The

results demonstrate that the shear flow generated by the rotating parallel disk can be used to measure cell adhesion and that the R_C can be clearly measured after testing.

It has been reported by LaPlaca & Thibault, Oztekin & Brown, Shouvelier & colleagues, and Shipman & colleagues that the shear flow generated by the rotating disk creates an inconsistent flow [28, 59-61]. It has been speculated that the irregularities in the flow would yield poor results and being unable to measure a well-defined radius of cells after testing. Their observation is based on the fact that the shear flow generated by the system used in this research is considered unstable. The identified instabilities are introduced secondary flows [28, 59-61] and the free energy at the PBS/air interface [61].

The primary flow is the one generated by the rotating disk, which is the one under study. A secondary flow is one that is superimposed on the primary flow. The work of Shouveiler and colleagues and that summarized by Oztekin and Brown demonstrated that a secondary flow forms at the fixed disk and travels upward in a spiral form [59, 60]. A secondary flow is undesirable because it affects the primary flow and in the case of cell adhesion would result in inconsistent critical radii. Several numerical solutions have been developed to correct the shear stress when a secondary flow is observed in the rotating parallel disk system [59-62].

The instability introduced by the free energy at the PBS/air interface was studied by Shipman and colleagues [61]. The flow properties depend on the shape of the liquid between the plates. The liquid can be concave (Figure 35a), convex (Figure 35b), or perfectly aligned with the disks (Figure 35c). This effect of free surface can be accounted for with a modification to the flow analysis [61]. However, the defects of the

edge shape can be ignored if the ratio of the disk gap to the disk radius is less than one ($H/R \ll 1$) for laminar or turbulent conditions. For the system under study, the highest H/R ratio is 0.04 for the chick embryo neuron cells on PDL coated glass. Therefore, the effect of the free energy at the PBS/air interface can be ignored in the analysis. Figure 35 illustrates the basic free surface geometries studied by Shipman and colleagues [61]. The shape used for this study is in the one shown in Figure 35b.

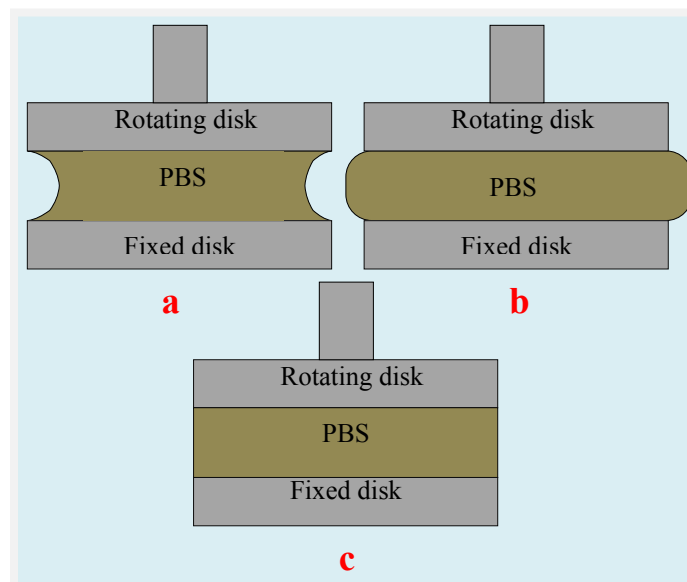


Figure 35 The instability introduced by the free energy at the PBS/air interface depends on the shape of the fluid (PBS).

Both instabilities have only been observed for turbulent flow and when the flow transitions from laminar to turbulent. A laminar flow is one where the particles in the flow move in smooth paths, in well defined concentric radius. The center of the flow is the same as the disks. Turbulent flow, however, has chaotic flow patterns [63].

In order to avoid instabilities, the flow required for the success of this study is a laminar flow. A laminar flow simplifies the analysis and calculation of the critical shear

stress of cell adhesion and ensures that no instabilities affect the flow. The Re , the Reynolds' number, for the rotational disk is defined as follows, where the ρ is the fluid density, ω angular velocity, H distance between disks, and μ viscosity [59-62].

$$Re = \frac{\rho\omega H^2}{\mu} \quad \text{Equation 1}$$

The transition from laminar to turbulent flow is determined when the dimensionless Reynolds (Re) number is less than 10 [26, 28, 59-62, 64-66]. The Re for all results presented in Chapter III are calculated and summarized below. The density of the PBS is approximately 1.0 g/ml and the other values are obtained from the test results of the rheometer. Table 11 summarizes the Re of the stable flow during testing of 3T3 fibroblasts and Table 12 lists the Re of the stable flow of the chick neuron cell culture.

Table 11 Reynolds number for test procedure used in NIH 3T3 Swiss mouse fibroblasts.

Sample	ω (rad/s)	H (μm)	μ (Pa.s)	Re
PMMA_25_03	22.0	480	0.026	0.195
Au/PVDF_20_01	18.5	480	0.006	0.710
PC_10_01	9.0	480	0.053	0.039

Table 12 Reynolds number for test procedure used in chick embryo retina neurons.

Sample	ω (rad/s)	H (μm)	$\mu \times 10^{-3}$ (Pa.s)	Re
S15_10	10.1	500	3.958	0.638
S16_25	20.6	500	4.854	1.061
S17_40	36.7	500	4.854	1.891
S19_55	50.5	500	4.358	2.897
S20_70	47.0	500	6.017	1.953
S24_25	21.7	500	4.609	1.177
S25_30	27.5	500	4.356	1.578

Figure 36 shows the Re for a S15_10 for the entire test. The plot indicates that the Re increases with time and all the values reported in Tables 11 and 12 are the maximum number. The Re changed throughout the test but was maintained below 10. This indicates that the rotational flow used in this analysis is entirely laminar. Additionally, the possibilities of having instabilities in the system due to turbulent flow or due to laminar to turbulent transition are null.

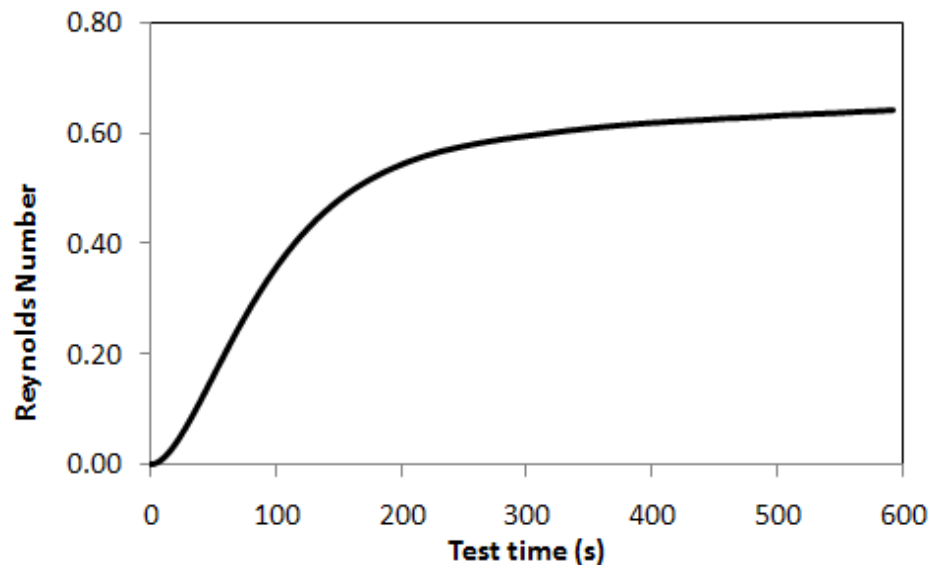


Figure 36 Reynolds number throughout test for S15_10. This shows the Re increases with time.

Another factor that disrupts the laminar flow is the surface roughness of the disks [60]. The disks used in this study are ground and polished to minimize the effects of surface roughness. The cells that are attached to the lower fixed plate introduce a roughness to the lower surface and might cause instabilities in the flow. Studies reported by Safran et al., however, indicate that the effects of surface roughness introduced by the cells attached to the fixed plate can be ignored since the cell height (~ 1 to $3 \mu\text{m}$) is

smaller than the distance between disks (500 μm maximum). The results reported by Safran and colleagues demonstrated that cells can be considered part of substrate and have an insignificant effect on the properties of the flow [67]. The present results showed that the laminar flow is not disrupted, not only because the $\text{Re} < 10$ throughout the test but because a well-defined R_C was measured after testing which indicate that the flow moves in well-defined circles as required for laminar flow.

Additionally, the measured μ is different for a cell cultured substrate and for a substrate with no cells, even if both are tested with the same τ_a . This variation in μ between cells and no cells on the substrate might already be accounting for the surface roughness introduced by the cells on the system but the introduced roughness is not enough to disrupt the laminar flow. Figure 37 shows the difference in measured viscosity for PMMA tested at $\tau_a = 25 \text{ dynes/cm}^2$ with and without cells. The PMMA with cells shows higher viscosity values than the PMMA sample without cells even though both samples were tested with the same controlled shear stress of 25 dynes/cm^2 .

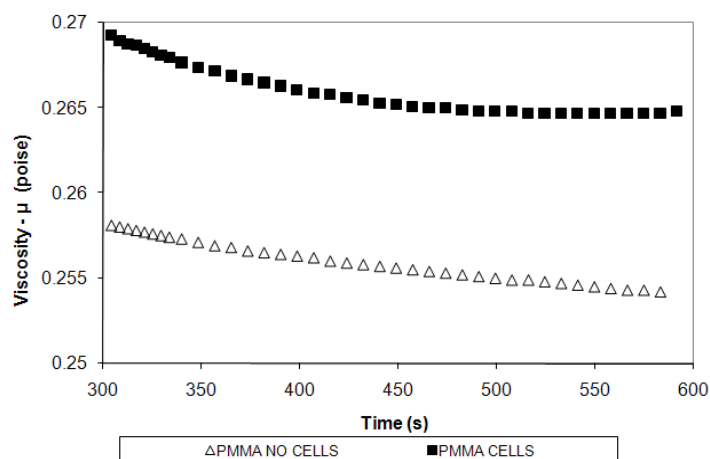


Figure 37 Difference in viscosity for sample of PMMA tested with and without cells at $\tau_a = 25 \text{ dynes/cm}^2$.

5.2. Critical shear stress

The results summarized in Tables 8 and 10 in Chapter IV demonstrate that the test provides a well-defined R_C . Except measuring the R_C only is not enough information. The same R_C can be obtained for samples with different cells and different substrate material when tested with different applied shear stress (τ_a). This can be observed in the results of PC_10_01 (3T3 fibroblasts on PC) and S19_55 (chick neurons on PDL/glass) which show 0.636cm and 0.631cm radii respectively. It is then necessary to calculate the shear stress at which the cells detached from the surface, the critical shear stress (τ_C). This can be accomplished by studying the flow properties.

The classical method for analysis of the laminar rotational flow is with the exact or the numerical solution of the Navier-Stokes equation in cylindrical coordinates. This equation represents the motion of a liquid or gas in time and space and is derived from a conservation of mass, flow, and energy in a system [28, 63]. Where, \vec{v} is the velocity profile in vector form, p is the pressure gradient, and g is the gravitational acceleration.

$$\rho \left(\frac{\partial \vec{v}}{\partial t} + \vec{v} \cdot \nabla \vec{v} \right) = -\nabla p + \rho \vec{g} + \mu \nabla^2 \vec{v} \quad \text{Equation 2}$$

Assuming constant density and that PBS is Newtonian, meaning its viscosity is constant for all applied shear strains, and the flow has reached steady state, the Navier-Stokes equation in cylindrical coordinates (r, θ, z) simplifies to Equation 3. Figure 38 shows the directions of the r, θ, z directions.

$$v_r \frac{\partial v_\theta}{\partial r} + \frac{v_r v_\theta}{r} + v_z \frac{\partial v_\theta}{\partial z} = v \left[\frac{\partial^2 v_\theta}{\partial r^2} + \frac{1}{r} \frac{\partial v_\theta}{\partial r} - \frac{v_\theta}{r^2} + \frac{\partial^2 v_\theta}{\partial z^2} \right] \quad \text{Equation 3}$$

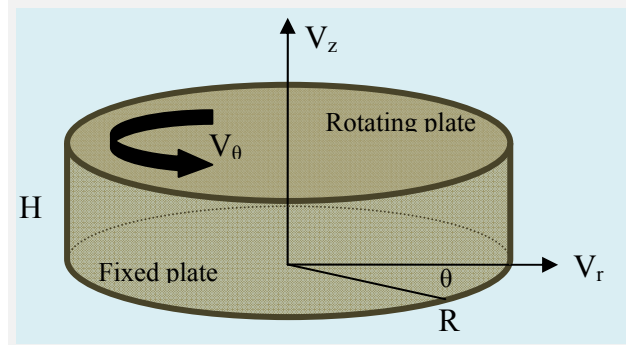


Figure 38 Schematic of parallel disk rotational flow in cylindrical coordinates (r, θ, z) . The total gap is H and the maximum radius is R .

Numerical solutions of this equation have been obtained [59-62, 65]. The exact solution to this partial differential equation has been found by LaPlaca and Thibault, Papadaki and McIntire, Ando et al., and Ono et al. [26, 28, 64, 66]. The exact solution is then used to find the shear stress at the fixed disk, which is the shear stress experienced by the cells. The shear stress in a laminar flow is a function of the viscosity (μ) of the system and the velocity gradient ($\partial\vec{v}/\partial z$) between the disks.

$$\tau = \mu \left(\frac{\partial\vec{v}}{\partial y} \right) \quad \text{Equation 4}$$

The velocity gradient is obtained from the Navier-Stokes equation in cylindrical coordinates. The equation can be simplified and substituted into equation 4 and results in:

$$\tau_{fixed\ disk} = \frac{\mu\omega r}{H} \quad \text{Equation 5}$$

Where ω is the angular velocity and is equal to v_θ , H is the distance between fixed and rotating disk and r is the radius. This equation can also be used to calculate the critical shear stress (τ_c). The μ , ω , and H are constant once the system reaches the steady state. Therefore, replacing the r for the R_c (critical radius) would provide the τ_c .

$$\tau_c = \frac{\mu\omega R_c}{H} \quad \text{Equation 6}$$

Equation 6 was used to calculate the τ_c of the samples with a well-defined R_c . The values of τ_c calculated for the 3T3 fibroblasts and the chick embryo neurons are summarized in Tables 13 and 14 respectively. The results of the chick embryo neurons are also shown graphically in Figure 39. The results indicate that the τ_c increases with increasing τ_a as well as with increasing radius. The results of S17_40 and S25_30 are the only two points that do not follow the curved trend. It was pointed out in the previous chapter that there was likely an error when measuring the R_c of S25_30 while the discrepancy in S17_40 was probably due to a miscalculation of the μ in the instrument. This will be further investigated in future study.

Table 13 The τ_c of NIH 3T3 Swiss mouse fibroblast on various surfaces.

Sample	R_c (cm)	ω (rad/s)	H (μm)	μ (Pa.s)	τ_c (dyne/cm^2)
PMMA_25_03	1.05	22.0	480	0.026	21.02
Au/PVDF_20_01	0.70	18.5	480	0.006	11.08
PC_10_01	0.636	9.0	480	0.053	5.09

Table 14 The τ_c of chick embryo neuron cells on poly-d-Lysine coated glass.

Sample	R_c (cm)	ω (rad/s)	H (μm)	$\mu \times 10^{-3}$ (Pa.s)	τ_c (dyne/cm^2)
S15_10	1.158	10.1	500	3.958	9.26
S16_25	0.976	20.6	500	4.854	19.52
S17_40	0.663	36.7	500	4.854	23.62
S19_55	0.631	50.5	500	4.358	27.76
S20_70	0.483	47.0	500	6.017	27.29
S24_25	0.933	21.7	500	4.609	18.66
S25_30	0.394	27.5	500	4.356	4.72

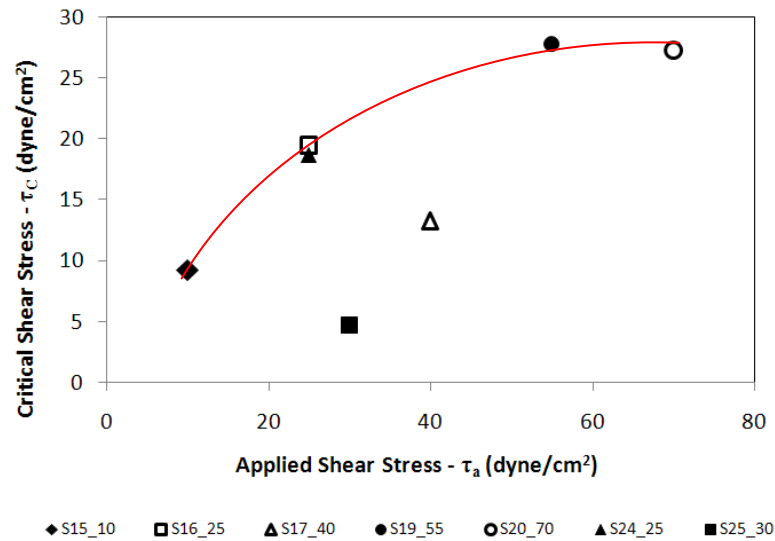


Figure 39 Results of chick embryo neurons on poly-D-lysine coated glass with traditional flow analysis.

Equation 6 can only be used if the system has reached a steady state and only if the fluid is Newtonian. The PBS used in this study is not Newtonian because the measured viscosity changes with varying shear strain. However, the measured μ remains constant once the flow is fully developed; this is at least the last 2 or 3 minutes of testing. For these reasons, a Newtonian fluid could be assumed for the analysis. Figures 40 and 41 show the viscosity and the angular velocity approach a constant value with increasing time for all samples.

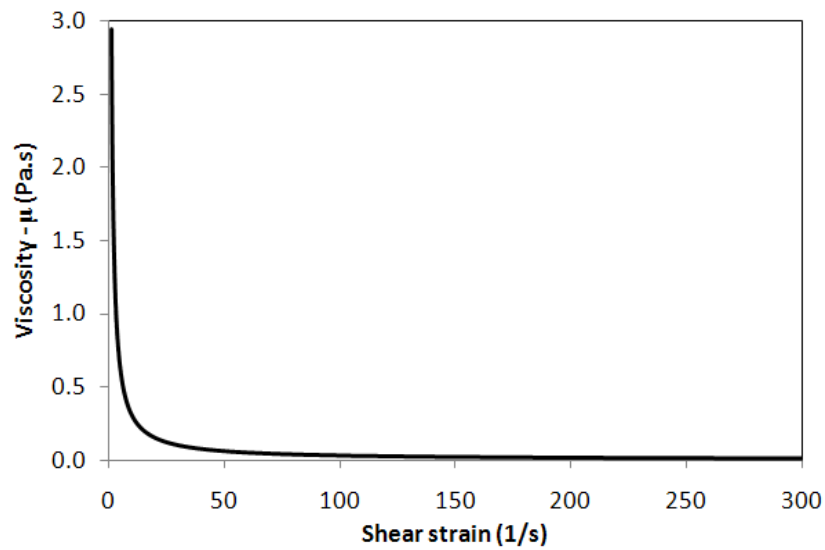


Figure 40 Viscosity vs. shear strain of PBS during S25_30 test. The changing viscosity with shear strain indicates PBS is not Newtonian.

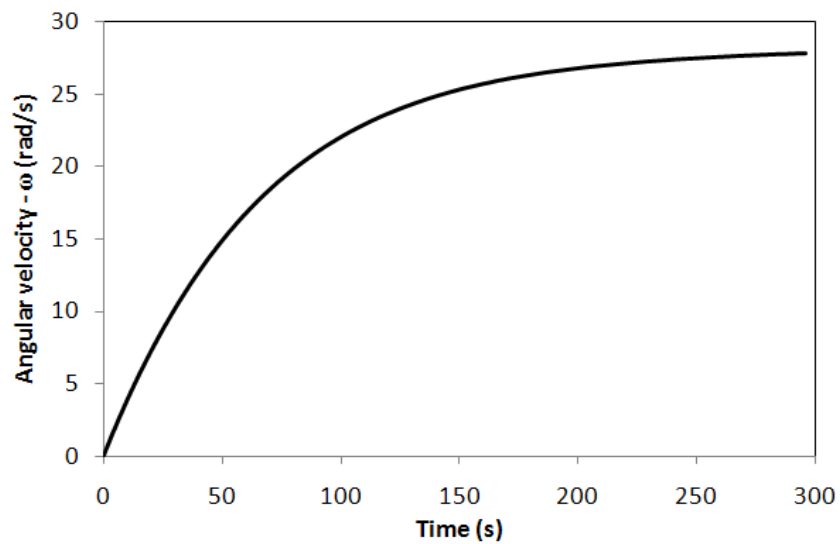


Figure 41 Angular velocity vs. test time of PBS during S25_30 test. The ω approaches a constant value.

Although the value measured for μ and ω change during the test, the instantaneous μ and ω are the same at all points along the radius. Using this principle the

μ , ω , and H are instantaneously the same for all points on the radius, including the maximum (R) and the critical (R_c). Solving for $\left(\frac{\mu\omega}{H}\right) = \frac{\tau_a}{R}$ from equation 3,

$$\left(\frac{\mu\omega}{H}\right)_{Applied} = \left(\frac{\mu\omega}{H}\right)_{at R_c} \quad \text{Equation 7}$$

This is true at any time during the test not only when the system reached equilibrium flow. This is equivalent to

$$\left(\frac{\tau_a}{R}\right)_{Applied} = \left(\frac{\tau_c}{R_c}\right)_{at R_c} \quad \text{Equation 8}$$

Finally, solving equation 6 for τ_c yields a function that is only dependent on R_a , R , and τ_a .

$$\tau_c = \tau_a \left(\frac{R_c}{R}\right) \quad \text{Equation 9}$$

Whenever a rotating parallel disk system is used, the shear stress is traditionally calculated with Equation 6 ($\tau_c = \frac{\mu\omega R_c}{H}$). This equation requires that μ , ω , H , and R_c be known to solve the shear stress at the fixed wall, or in this case the τ_c . On the other hand, finding τ_c with equation 9, $\tau_c = \tau_a \left(\frac{R_c}{R}\right)$, only requires measuring R_c . The two results are compared to verify if simplified equation 9 can be used to determine the τ_c for the proposed cell adhesion method. Tables 15 and 16 summarize the τ_c calculated with Equation 9 for 3T3 fibroblasts and chick neurons respectively. Figure 42 shows graphically the results obtained for the chick neuron samples. It is important to note that S17_40 follows the increasing trend like the other samples, unlike in Figure 39 because the μ is not used to calculate the τ_c . The results are in good agreement with those obtained with the traditional flow analysis shown in Tables 13 and 14.

Table 15 The τ_c of 3T3 fibroblast on various surfaces with proposed analysis.

Sample	τ_{applied} (dyne/cm ²)	Rc (cm)	τ_c (dyne/cm ²)
PMMA_25_03	25	1.05	21.0
Au/PVDF_20_01	20	0.70	11.2
PC_10_01	10	0.636	5.088

Table 16 The τ_c of chick neuron cells on PDL coated glass with proposed analysis.

Sample	τ_{applied} (dyne/cm ²)	Rc (cm)	τ_c (dyne/cm ²)
S15_10	10	1.158	9.26
S16_25	25	0.976	19.53
S17_40	40	0.663	21.2
S19_55	55	0.631	27.76
S20_70	70	0.483	27.05
S24_25	25	0.933	18.66
S25_30	30	0.394	3.935

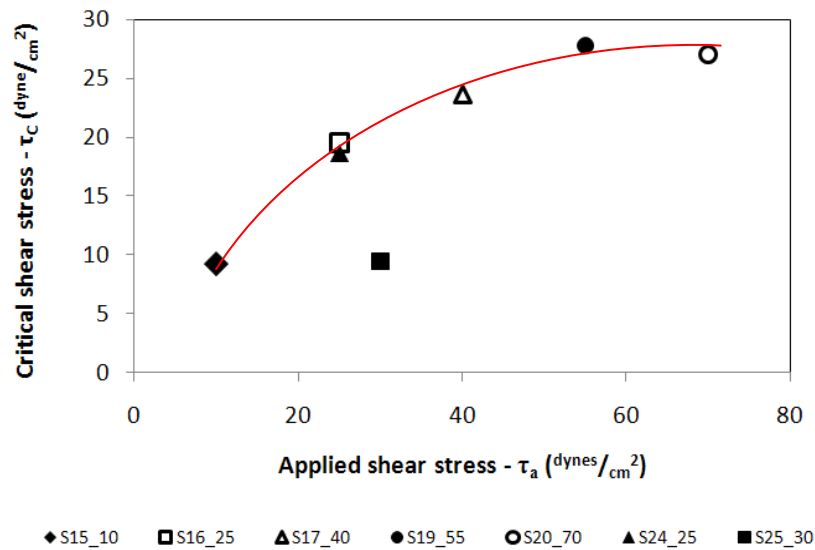


Figure 42 Results of chick embryo neurons on poly-D-lysine coated glass with simplified equation.

The results obtained with both flow analysis methods must be compared to assess the reliability of the proposed and simplified analysis. These values are compared in Tables 17 and 18 for 3T3 and in Figures 43 and 44 for fibroblasts and chick neurons respectively. The discrepancy of the two methods is quantified with a % difference between the calculated τ_c .

Table 17 The % difference between traditional and proposed analyses for 3T3 fibroblast.

Sample	$\tau_c = \frac{\mu\omega R_c}{H}$ Eq. 9 (dyne/cm ²)	$\tau_c = \tau_a \left(\frac{R_c}{R}\right)$ Eq. 6 (dyne/cm ²)	% difference
PMMA_25_03	21.02	21.0	0.10%
Au/PVDF_20_01	11.08	11.2	1.07%
PC_10_01	5.09	5.088	0.04%

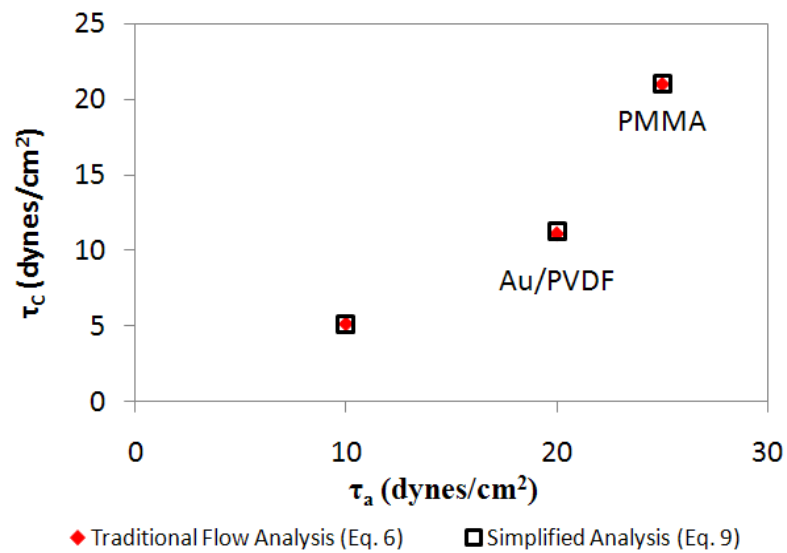


Figure 43 Comparison of traditional flow analysis and simplified flow analysis for 3T3 fibroblasts.

Table 18 The % difference between traditional and proposed analyses for chick neurons on PDL coated glas.

Sample	$\tau_c = \frac{\mu\omega R_c}{H}$ Eq. 9 (dyne/cm^2)	$\tau_c = \tau_a \left(\frac{R_c}{R}\right)$ Eq. 6 (dyne/cm^2)	% difference
S15_10	9.26	9.26	0%
S16_25	19.53	19.52	0.05%
S17_40	21.2	23.62	10.25%
S19_55	27.76	27.76	0%
S20_70	27.05	27.29	0.92%
S24_25	18.66	18.66	0%
S25_30	3.935	4.72	16.63%

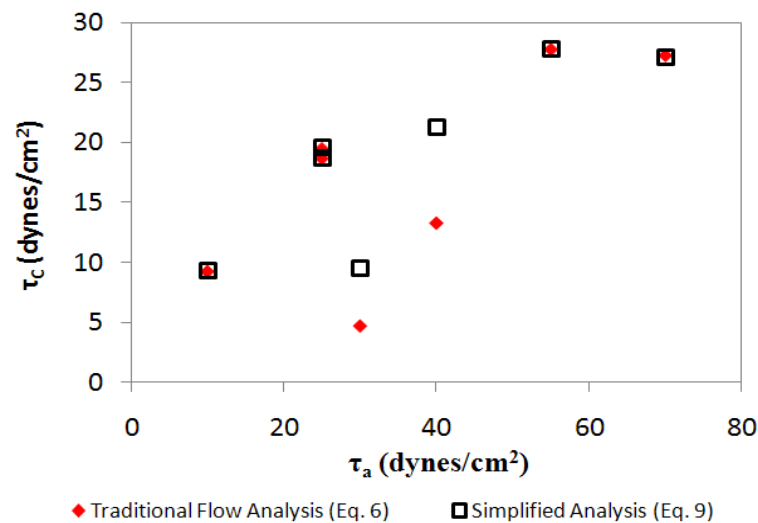


Figure 44 Comparison of traditional flow analysis and simplified flow analysis for chick embryo neuron samples.

With the exception of S17_40 and S25_30, the proposed analysis of τ_c closely agrees with the traditional fluid analysis method. However, it was previously noted that S25_30 has the possibility of incorrect R_c measurement and S17_40 has the possibility of incorrect μ measurement by the rheometer. Furthermore, the proposed analysis has the advantage that only one variable must be measured after the test (R_c) and that the

flow system does not need to reach equilibrium for the equation to apply. This simplification, however, only applies if the applied shear stress is the controlled variable during the test.

5.3. Effects of cell elasticity on R_c and τ_c

Many cell and tissue properties can be imitated by biomaterials but there is still more work to be done to fully imitate the tissue and cell response. This is because cells are live organisms that adapt and respond to their environment and the aspect of cell adhesion is not the exception. The internal components of a cell control its elastic properties by rearranging into different structures [24, 67, 68].

Cells that attach to a surface experience normal and lateral forces. The normal forces (F_N) are due to van der Waals interaction between the cell and the substrate, which means they are weaker than lateral forces (F_L). The F_L are due to stretching of the fibroblast as it attaches to the substrate. The F_N is measured with AFM by pulling the cell from the substrate material. The measured values are in the order of a few picoNewtons to nanoNewtons. The F_L controls cell size and shape. The cells can easily adjust their F_L depending on the stimulus from the environment [24, 67]. The F_N and F_L of neuron cells are lower than those of fibroblasts [68]. Measuring the shear stress necessary to detach the cells from the substrate (τ_c) is analogous to measuring the F_L of the cell-substrate pair. Figure 45 shows the diagram of the F_N and F_L on an attached cell. Other factor that affects the F_N is gravity but its contribution is minimum and can be ignored [61].

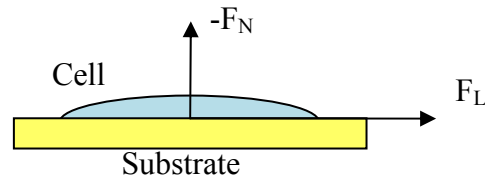


Figure 45 Schematic of normal (F_N) and lateral forces (F_L) acting on an attached cell.

The cell response to external stimulus was observed for the chick embryo neuron cells in this study. The calculated critical shear stress increased with increasing applied shear stress as can be observed in Figure 42. This increase is due to the cell response to the applied deformation from the shear flow. This indicates that the F_L increase due to the forces applied to the cells by the flow. It can also be observed that the critical shear stress reaches a plateau and stabilizes after an applied shear stress of 55 dynes/cm^2 which translates to a critical shear stress of approximately 27 dynes/cm^2 . The plateau indicates that the cell's elastic limit has been reached. The cell adhesion strength cannot be adjusted any more and the cells detach from the surface.

According to the results shown in Table 18 and in Figure 42, as well as observation of the critical radii for all samples, a cell detachment process is proposed in Figure 46. Once the cell elastic limit has been reached, the proteins that connect the cell to the substrate begin to break off. Figure 46 illustrates how the cells begin detachment from the substrate when a flow is applied. The protein connections begin breaking slowly until the entire cell is removed. This would indicate that the cells behave elastically. As a matter of fact, Zhu et al. and Safran et al. reported that due to the elastic response of cells, an applied deformation would align the cells in the direction of

deformation [24, 67]. Each cell type has different elastic behavior and, depending on the cell and the strength of applied deformation, the cells may align in the direction of applied deformation, change in shape, or detach.

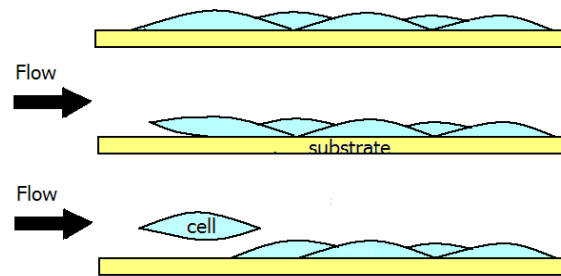


Figure 46 Steps for cell detachment when exposed to a shear flow.

In the case of 3T3 fibroblasts, no cell alignment or shape change was observed. For the studies conducted on chick neurons, no cell shape or density change was observed before and after testing. Figure 47a shows the cell culture on S15_10 before testing and Figure 47b shows the cell culture after testing. Both images show the same cell size, similar size cell groups, and similar cell density on the surface and were taken with the same magnification. Cell culture images of chick neuron cultures from before and after testing are shown in Appendix A for other samples.

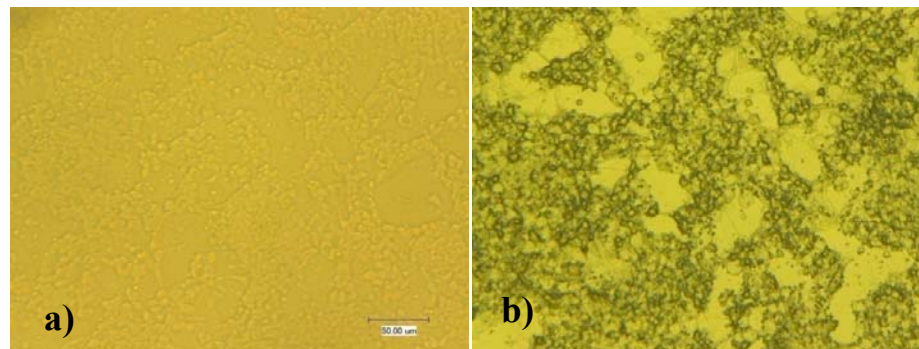


Figure 47 Images of S16_25 before and after testing. Cell shape and density inside the Rc was not affected by the shear flow.

Cell alignment was reported in several adhesion studies. Never the less, in the present research, cell alignment was not observed for either cell culture because the testing time was only 10 minutes and because the cells are tested after 24 hours of cell seeding. This makes a difference because cells generally attach in 2 hours. Alignment was only observed for PDL proteins on the glass substrate. Figure 48 shows protein alignment on S16_25 in the direction of the flow. The radius of the sample is on the far right and the edge is on the left as shown.

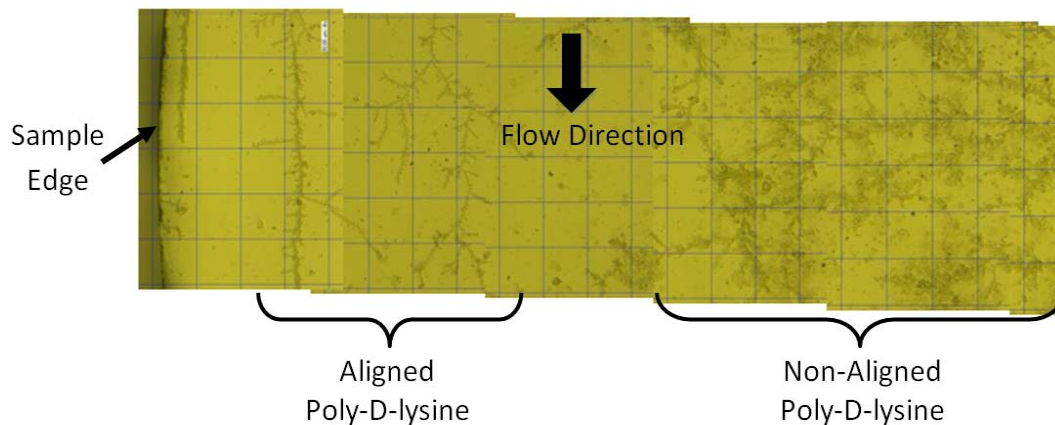


Figure 48. The poly-D-lysine proteins show alignment after testing in the flow direction.

5.4. Effect of substrate material on R_C and τ_C

Surface energy, surface roughness, chemistry, and elastic properties of the substrate material also play a significant role in the adhesion strength of cells. Surface energy is a way to quantify for the open bonds of the molecules on the substrate's surface. High surface energy promotes cell adhesion [46, 69, 70] because cell adhesion proteins will create stronger connections between the substrate and the cell.

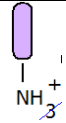
High surface roughness has been shown to promote cell adhesion for polymers, metals, and ceramic materials [46, 69-72]. Surface roughness promotes cell adhesion for two reasons. The first reason is if the vertical deviations of the surface (peak-to-valley) are higher than the cell height, the cells will fall inside the valleys and be protected from any external flow or forces applied on the surface. The second, and the most important reason, is that having a high surface roughness indicates extra surface area, which show increased surface energy. Table 19 lists the surface roughness of the substrates used in this study for 3T3 fibroblasts and chick neuron cells. The surface roughness (Ra) was measured with a TR200 Profilometer from Qulitest.

Table 19 The average surface roughness (Ra) of materials.

Substrate	Cells	Ra (μm)	Std Dev
PMMA	Fibroblasts	0.005	0.0007
Au coated PVDF	Fibroblasts	1.113	0.0778
PC	Fibroblasts	0.017	0.0064
Glass	Chick neurons	0.037	0.0315

Substrate chemistry also plays an important role in cell adhesion. As mentioned in the Chapter I, cells attach to external surfaces through adhesion proteins. The adhesion proteins for fibroblasts are mainly fibronectin and the adhesion protein for the chick neurons is PDL. In general, proteins have electropositive open ends. Therefore, a more electronegative surface will have a tendency to show higher adhesion strength. Metallic materials show an adhesion strength of 1 or 2 orders of magnitude higher than polymeric materials [46]. This is due to the electron cloud in the material which makes the surface more electronegative. The polymer chemical structure and the adhesion proteins used in this study are shown in Table 20.

Table 20 Chemical structure of the polymers used as substrates for NIH 3T3 Swiss mouse fibroblast cultures.

Substrate / Cell	Chemical structure	Adhesion Protein
PMMA / Fibroblast	$\left[\begin{array}{c} \text{H} \quad \text{CH}_3 \\ \quad \\ -\text{C}-\text{C}- \\ \quad \\ \text{H} \quad \text{C}=\text{O}-\text{O}-\text{CH}_3 \end{array} \right]_n$	 Fibronectin
PC / Fibroblast	$\left[\text{O}-\text{C}_6\text{H}_4-\text{C}(\text{CH}_3)(\text{C}_6\text{H}_4)-\text{O}-\text{C}(=\text{O}) \right]_n$	Ibid
Au-PVDF / fibroblasts	$\left[\begin{array}{c} \text{H} \quad \text{F} \\ \quad \\ -\text{C}-\text{C}- \\ \quad \\ \text{H} \quad \text{F} \end{array} \right]_n$	Ibid
Glass / chick embryo neurons	--	Poly-D-lysine $\text{OH}-\overset{\text{O}}{\parallel}{\text{C}}-\underset{\text{NH}_2}{\text{CH}}-\text{CH}_2-\text{CH}_2-\text{CH}_2-\text{CH}_2-\text{NH}_2$

PMMA has an electron pump in the CH₃ of the carboxylic (COOH) side that travels through the carboxylic structure and helps open one oxygen bond (Figure 49a). The released electron then reacts with the NH₃ at the end of the fibronectin which gives up an electron and becomes NH₂⁺ (Figure 49b). The open oxygen bond from the PMMA then connects with the NH₂⁺ from the fibronectin forming a primary bond between the PMMA substrate and the fibronectin. The electron pump in PMMA makes it more electronegative which promotes cell adhesion. Figure 49 shows the reaction mechanisms for the attachment of fibronectin to PMMA.

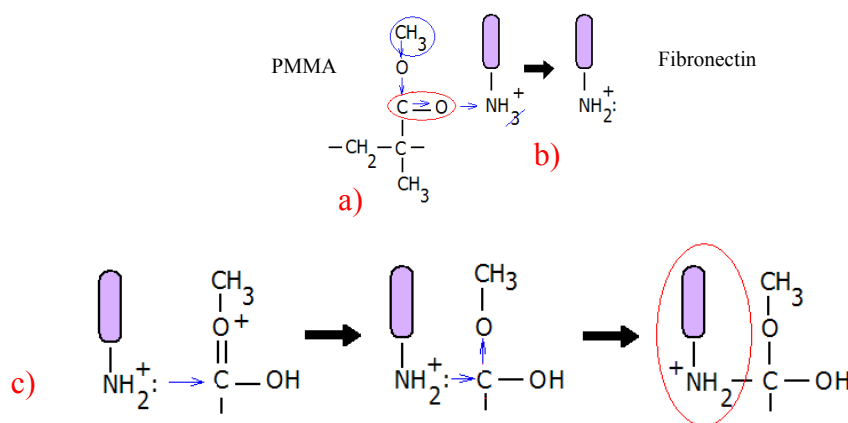


Figure 49 Reaction mechanisms for fibronectin and PMMA.

For PC, unlike PMMA, there is no electron pump in the structure. In addition, any electrons are free to travel through the backbone due to the oxygen links. This gives PC a lower surface electronegativity than PMMA. This helps explain why PMMA has a critical shear stress of 21.0 dynes/cm² while PC only have adhesion strength of 5.09 dynes/cm², almost four times lower.

Based on the results the effect of surface roughness on cell adhesion is not as dominant as that of the substrate chemistry. Surface roughness can help fine-tune adhesion to the required value but surface chemistry is a key factor.

The adhesion strength of gold coated PVDF is 11.1 dynes/cm². Since the coating is metallic, a high adhesion strength would be expected as shown in the literature for other metallic materials. This behavior was also observed by McMillan and colleagues for a gold coated polyurethane sample [73]. Gold gets contaminated within milliseconds of exposure to the environment which lowers cell adhesion. In addition, liquid solutions, such as the cell culture media and the PBS used for testing tend to form microcracks in the gold coating exposing the cells to the polymer, in this case PVDF [73]. Therefore,

parts of the cells attach to the PVDF and parts of the cells attach to the gold and the measured value is a mixture of the adhesion of cells on gold and of the adhesion of cells on the PVDF. All this yields a lower cell adhesion value than for most metallic materials.

The adhesion molecule for chick embryo neuron cells is PDL. The glass substrates were coated prior to cell culture. PDL was specifically engineered to promote neuron adhesion to any substrate. Therefore, any surface coated with PDL guarantees good adhesion.

Another factor that affects cell adhesion is the mechanical properties of the substrate. When a force or deformation is applied to a material, the material will tend to deform. This would affect the cell adhesion because the applied force on the material would be translated to the cell [24]. This, however, is not an issue in this study since the substrate material remains intact throughout the test. No external forces are applied on the substrate and therefore the cells are not affected by the elastic response of the substrate.

CHAPTER VI

CONCLUSIONS

This research investigated the adhesion mechanisms between cells and materials. A rotating parallel disk was used to measure cell adhesion. One disk is fixed while the other rotates generating a shear flow. Results showed that the shear stress experienced by the cells varied with radial location, being the highest at the edge and zero at the disk's center. There was a critical point along the radius where the shear stress experienced by the cells equals their adhesion strength. The cells outside this radius were removed and the cells inside it remained attached to the surface. The proposed methodology was proven to provide reliable adhesion measurements to a wide variety of cell types and material substrates. This allows to quantify and compare the biocompatibility of many materials *in vitro*.

The flow analysis to calculate the adhesion shear stress is simplified with the proposed methodology because the shear stress generated by the rotating disk can be precisely controlled. This simplified analysis is in good agreement with the traditional flow analysis. The proposed analysis applies only to laminar flow conditions which can be controlled by adjusting the angular velocity of the rotating disk, by adjusting the distance between disks, or by using a testing media with different viscosity. In addition, optimum results are obtained when approximately 70% of the substrate material is covered with cells.

The proposed methodology for measuring cell adhesion to substrates showed repeatable results. Cell adhesion is a key aspect of cell communication and function and

could be used to quantify the biocompatibility of materials. There are two major conclusions in this research; cell adhesion strength greatly depends on the substrate material and cells adjust their adhesion strength depending on the environment that surrounds them.

Cell adhesion depends on the chemistry and the surface energy of the material. Material chemistry plays an important role because a more electronegative material shows higher cell adhesion. This behavior is due to the electropositive nature of the adhesion proteins that connect the cells to the materials. These results were observed from the NIH 3T3 Swiss mouse fibroblasts cultured on PMMA, PC and gold coated PVDF. The adhesion shear stress for fibroblasts was 21.0 dynes/cm² on PMMA, 5.09 dynes/cm² on PC, and 11.1 dynes/cm² on gold coated PVDF. It was shown in Chapter V that PMMA is more electronegative than PC resulting in fibroblast adhesion to PMMA four times higher than the adhesion to PC. It would be expected that a metallic material, such as the gold coating on PVDF, would be higher; however, gold is contaminated within fractions of a second of contact with the environment resulting in lower adhesion strengths. Higher surface energy of the material also increases the adhesion strength of the material because higher surface energy allows more adhesion proteins to attach to the surface. More adhesion proteins indicate a stronger connection between the cells and the material's surface.

The internal components of cells realign to adjust the adhesion strength of the cell. This is a natural cell response to external stimulus. In this study, the external stimulus is generated by the shear stress and cell adhesion strengthens when the applied

shear stress increases. This behavior was observed for the chick embryo neuron cells cultured on poly-D-lysine coated glass. The critical shear strength of adhesion was 9.26 dynes/cm² with an applied 10 dynes/cm² and the critical shear strength of adhesion was 27.0 dynes/cm² when the applied shear stress was 70 dynes/cm². The cells, however, reach an elastic limit and do not strengthen any further. The elastic limit of cell adhesion for chick embryo neurons was reached after an applied 55 dynes/cm² or higher which resulted in ~27 dynes/cm² adhesion shear stress.

Additionally, the results obtained for the NIH 3T3 Swiss mouse fibroblasts cultured on PMMA, PC and gold coated PVDF demonstrate that the system can be used to quantify and compare the cell adhesion to different materials. The results obtained for the chick embryo neuron cells on poly-D-lysine coated glass demonstrate the reliability and repeatability of the system.

The results of this research indicate that higher adhesion strengths will be obtained for materials with higher electronegativity. The adhesion strength can also be adjusted by controlling the surface energy of the material, which can be fine-tuned by controlling the surface roughness where higher surface roughness gives more surface and consequently more surface energy.

The cell adhesion method proposed in this study could significantly impact the design and fabrication of artificial implants and could allow considerable improvement in their design and lifetime. Knowing the cell-material adhesive strength can help in material selection for specific biological applications. If the adhesive strength between a healthy bone and the tissue surrounding it is known, the material selected for an artificial

joint can also be selected or optimized to achieve the same adhesive strength between the biomaterial and the healthy tissue. Because the tissue behavior is less disrupted, this might result in improved biocompatibility and increase the life of the implant.

Ultimately, this methodology could be used to quantify how material processing and surface treatment of finished or nearly finished artificial implants affect cell adhesion and their biocompatibility.

6.1. Future recommendations

Future studies are recommended to further understand the effect of surface roughness on cell adhesion. Other polymeric surfaces with higher polarities than PMMA, as well as metallic and ceramic materials should be used. For the case of protein coated surfaces, the effect of protein molecular weight and % surface coverage should be assessed.

REFERENCES

- [1] K.C. Dee, D.A. Puleo and R. Bizios, *An introduction to tissue-biomaterial interactions*, John Wiley & Sons, Hoboken, New Jersey, 2002.
- [2] R. Sivakumar, On the relevance and requirements of biomaterials, *Bulletin of Materials Science*, **22** (1999), 647-655.
- [3] A. Piezoferrato, G. Ciapetti, S. Stea, E. Cenni, C.R. Arciola, D. Granchi and L. Savarino, Cell culture methods for testing biocompatibility, *Clinical Materials*, **15** (1994), 173-190.
- [4] D. Williams, Revisiting the definition of biocompatibility, *Medical Device Technology*, **14** (2003), 10-13.
- [5] C.J. Kirkpatrick, F. Bittinger, M.Wagner, H.Koehler, T.G.v. Kooten, C.L. Klein and M. Otto, Current trends in biocompatibility testing *Proceedings Institution of Mechanical Engineers*, **212** (1998), 75-84.
- [6] P.-H. Puecha, K. Poole, D. Knebelc and D.J. Muller, A new technical approach to quantify cell-cell adhesion forces by AFM, *Ultramicroscopy*, **106** (2006), 637-644.
- [7] E. Martines, K. McGhee, C. Wilkinson and A. Curtis, A Parallel-plate flow chamber to study initial cell adhesion on a nanofeatured surface, *IEEE Transactions on Nanobioscience*, **3** (2004), 90-96.
- [8] L. Hu, X. Zhang and P. Miller, Cell adhesion measurement by laser-induced stress waves, *Journal of Applied Physics*, **100** (2006), 84701-84705.
- [9] A.J. Garcia, P. Ducheyne and D. Boettiger, Quantification of cell adhesion using a spinning disc device and application to surface-reactive materials, *Biomaterials*, **18** (1997), 1091-1098.
- [10] A.A. Anderson, A hybrid mathematical model of solid tumour invasion: the importance of cell adhesion, *Mathematical Medicine and Biology*, **22** (2005), 163-186.
- [11] A.S.G. Curtis and J.M. Lackie, *Measuring Cell Adhesion*, John Wiley & Sons, New York, 1991.
- [12] A. Yamamoto, S. Mishima, N. Maruyama and M. Sumita, Quantitative evaluation of cell attachment to glass, polystyrene, and fibronectin- or collagen-coated polystyrene by measurement of cell adhesive shear force and cell

- detachment energy, *Journal of Biomedical Material Research*, **50** (2000), 114–124.
- [13] A.L. Kierszenbaum, *Histology and Cell Biology: An Introduction to Pathology*, Mosby, St. Louis, Missouri, 2002.
- [14] T.D. Pollard and W.C. Earnshaw, *Cell Biology*, Saunders, Philadelphia, PA, 2002.
- [15] B. Alberts, D. Bray, J. Lewis, M. Raff, K. Roberts and J.D. Watson, *Molecular Biology of The Cell*, Garland Publishing, New York, 1994.
- [16] L.-H.E. Hahn and K.M. Yamada, Isolation and Biological Characterization of Active Fragments of the Adhesive Glycoprotein Fibronectin, *Cell*, **18** (1979), 1043-1 1051.
- [17] A. Woods, J.R. Couchman, S. Johansson and M. Hook, Adhesion and cytoskeletal organisation of fibroblasts in response to fibronectin fragments, *The EMBO Journal*, **5** (1986), 665-670.
- [18] M.M. Lotz, C.A. Burdsal, H.P. Erickson and D.R. McClay, Cell adhesion to fibronectin and tenascin: quantitative measurements of initial binding and subsequent strength and response, *The Journal of Cell Biology*, **109** (1989), 1795-1805.
- [19] W. Banes, D.A. Sirbasu and G.H. Sato, *Methods for Preparation of Media, Supplements, and Substrata for Serum-free Animal Cell Culture*, N.R. Liss, New York, 1984.
- [20] Y.J. Kim, J.-W. Shin, K.D. Park, J.W. Lee, N. Yui, S.A. Park, K.S. Jee and J.K. Kim, A study of compatibility between cells and biopolymeric surfaces through quantitative measurements of adhesive forces, *Journal of Biomaterials Science and Polymer Education*, **14** (2003), 1311– 1321.
- [21] S.L. Ishaug, G.M. Crane, M.J. Miller, A.W. Yasko, M.J. Yaszemski and A.G. Mikos, Bone formation by three-dimensional stromal osteoblast culture in biodegradable polymer scaffolds, *Journal of Biomedical Materials Research*, **36** (1997), 17-28.
- [22] H. Lu, L.Y. Koo, W.M. Wang, D.A. Lauffenburger, L.G. Griffith and K.F. Jensen, Microfluidic shear devices for quantitative analysis of cell adhesion, *Analytical Chemistry*, **75** (2004), 5257-5264.

- [23] L.S. Channavajjala, A. Eidsath and W.C. Saxinger, A simple method for measurement of cell-substrate attachment forces: application to HIV-1 Tat, *Journal of Cell Science*, **110** (1997), 249-256.
- [24] C. Zhu, G. Bao and N. Wang, Cell mechanics: mechanical response, cell adhesion, and molecular deformation, *Annual Review of Biomedical Engineering*, **2** (2000), 189-226.
- [25] M.H. Buschmann, P. Dieterich, N.A. Adams and H.J. Schnittler, Analysis of flow in a cone-and-plate apparatus with respect to spatial and temporal effects on endothelial cells, *Biotechnology and Bioengineering*, **89** (2005), 493-502.
- [26] O. Ono, J. Ando, A. Kamiya, Y. Kuboki and H. Yasuda, Flow effects on cultured vascular endothelial and smooth muscle cell functions, *Cell Structure and Function*, **16** (1991), 365-374.
- [27] C.P.M. Reutelingsperger, R.G.J.V. Gool, V. Heijnen, P. Frederik and T. Lindhout, The rotating disc as a device to study the adhesive properties of endothelial cells under differential shear stresses, *Journal of Materials Science: Materials in Medicine*, **5** (1994), 361-367.
- [28] M.C. LaPlaca and L.E. Thibault, An in vitro traumatic injury model to examine the response of neurons to a hydrodynamically-induced deformation, *Annals of Biomedical Engineering*, **25** (1997), 665-677.
- [29] M. Benoit, D. Gabriel, G. Gerisch and H.E. Gaub, Discrete interactions in cell adhesion measured by single-molecule force spectroscopy, *Natural Cell Biology*, **2** (2000), 313-317.
- [30] N. Pyo, S. Tanaka, C.E. McNamee, Y. Kanda, Y. Fukumori, H. Ichikawa and K. Higashitani, Effect of the cell type and cell density on the binding of living cells to a silica particle: an atomic force microscope study, *Colloids and Surfaces B: Biointerfaces*, **53** (2006), 278-287.
- [31] G. Sagvolden, I. Giaever, E.O. Pettersen and J. Feder, Cell adhesion force microscopy, *Proceedings of the National Academy of Sciences: Biophysics*, **96** (1999), 471-476.
- [32] J.-Y. Shao and R.M. Hochmuth, Micropipette suction for measuring piconewton forces of adhesion and tether formation from neutrophil membranes, *Biophysical Journal*, **71** (1996), 2892-2901.
- [33] K.J. Bundy, L.G. Harris, B.A. Rahn and R.G. Richards, Measurement of fibroblast and bacterial detachment from biomaterials using jet impingement, *Cell Biology International*, **25** (2001), 289-307.

- [34] P. Bongrand, P.M. Claesson and A.S.G. Curtis, *Studying Cell Adhesion*, Springer - Verlag Berlin Heidelberg, Berlin, Germany, 1994.
- [35] T. Ushida, M. Nakayama and T. Tateishi, Cell adhesion strength to biomaterials and influence of fibronectin, *Advanced Biomaterials*, **10** (1992), 99-103.
- [36] F. Ming, W.J.D. Whish, J. Hubble and R. Eiseenthal, Estimation of parameters for cell surface interactions: maximum binding force and detachment constant, *Enzyme and Microbial Technology*, **22** (1998), 94-99.
- [37] T.D. Brown, Techniques for mechanical stimulation of cells in vitro: a review, *Journal of Biomechanics*, **33** (2000), 3-14.
- [38] B.R. Blackman, K.A. Barbee and L.E. Thibault, In vitro cell shearing device to investigate the dynamic response of cells in a controlled hydrodynamic environment, *Annals of Biomedical Engineering*, **28** (2000), 363–372.
- [39] A.M. Malek, R. Ahlquist, G.H. Gibbons, V.J. Dzau and S. Izumo, A cone-plate apparatus for the in vitro biochemical and molecular analysis of the effect of shear stress on adherent cells, *Methods in Cell Science*, **17** (1995), 165-176.
- [40] H.-J. Schnittler, R.P. Franke, U. Akbay, C. Mrowietz and D. Drenckhahn, Improved in vitro rheological system for studying the effect of fluid shear stress on cultured cells, *American Journal of Physiology*, **256** (1993), C289-C298.
- [41] R.M. Hakim, R.L. Wingard and R.A. Parker, Effect of the dialysis membrane in the treatment of patients with acute renal failure, *The New England Journal of Medicine*, **331** (1994), 1338-1342.
- [42] S.M. Lang and H. Schiffel, Effect of dialyser biocompatibility on recovery from acute renal failure after cadaveric renal transplantation *Nephrology Dialysis Transplantation*, **15** (2000), 134-135.
- [43] S.A. Alonso, J. Lau and B.L. Jaber, Biocompatible hemodialysis membranes for acute renal failure (review), in: *Cochrane Database of Systematic Reviews* Vol. CD005283, 2008, pp. 1-38.
- [44] G.J. Todaro and H. Green, Quantitative studies of the growth of mouse embryo cells in culture and their development into established lines, *The Journal of Cell Biology*, **17** (1963), 299-313.
- [45] C. O'Neill, P. Jordan and G. Klandt, Evidence for two distinct mechanisms of anchorage stimulation in freshly explanted and 3T3 Swiss mouse fibroblasts, *Cell*, **44** (1986), 489-496.

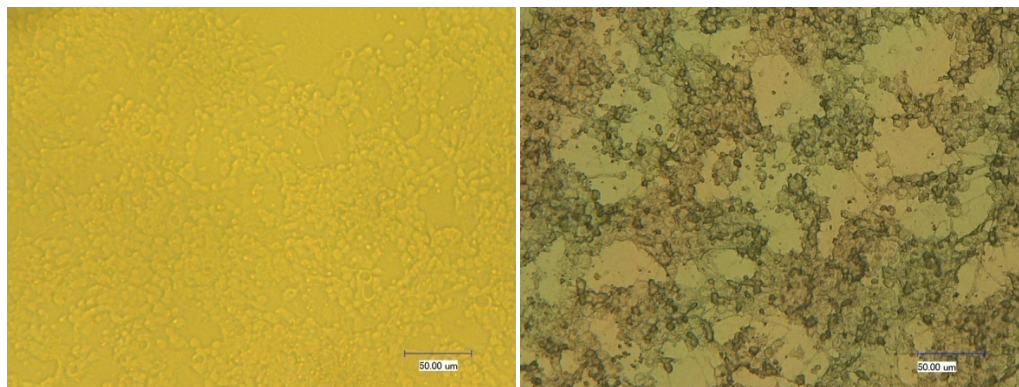
- [46] N.J. Hallab, K.J. Bundy, K. O'Connor, R.L. Moses and J.J. Jacobs, Evaluation of metallic and polymeric biomaterial surface energy and surface roughness characteristics for directed cell adhesion, *Tissue Engineering*, **7** (2001), 55-71.
- [47] Albino swiss mouse embryo fibroblasts (3T3 Line), in: *Live-Cell Imaging: Cell Motility*, Nikon MicroscopyU, Melville, NY 2008.
- [48] A. Moscona, Rotation-mediated histogenetic aggregation of dissociated cells, *Experimental Cell Research* **22** (1960), 455-475.
- [49] G. Ko, Ko, Michel, Dryer, Stuart E., Circadian regulation of cGMP-gated cationic channels of chick retinal cones: erk MAP kinase and Ca²⁺/calmodulin-dependent protein kinase II, *Neuron*, **29** (2001), 12.
- [50] G.Y.P. Ko, M.L. Ko and S.E. Dryer, Circadian phase-dependent modulation of cGMP-gated channels of cone photoreceptors by dopamine and d2 agonist, *The Journal of Neuroscience*, **23** (2003), 3145-3153.
- [51] R. Dubelcco and M. Vogt, Plaque formation and isolation of pure lines with poliomyelitis viruses, *Journal of Experimental Medicine*, **99** (1954), 167-182
- [52] J.T. Best, Revision Total hip and total knee arthroplasty, *Orthopaedic Nursing*, **24** (2005), 174-181.
- [53] T. H. Huang, J.-J. Yang, H. Li and C.-T. Kao, The biocompatibility evaluation of epoxy resin-based root canal sealers in vitro, *Biomaterials*, **23** (2002), 77-83.
- [54] G. Laroche, Y. Marois, R. Guidoin, M.W. King, L. Martin, T. How and Y. Douville, Polyvinylidene fluoride (PVDF) as a biomaterial: from polymeric raw material to monofilament vascular suture, *Journal of Biomedical Materials Research*, **29** (1995), 1525-1536.
- [55] M.C. Cortizo, M.F.L.d. Mele and A.M. Cortizo, Metallic dental material biocompatibility in osteoblastlike cells, *Biological Trace Element Research*, **100** (2004), 151-168.
- [56] Axiovert 200 MAT, in: *Inverted Microscopes Vol. 2008*, Germany, 2008.
- [57] Texas A&M University. Microscopy & Imaging Center, in: *JEOL JSM-6400 Scanning Electron Microscope Vol. 2008*, College Station, TX, 2008.
- [58] C.W. Macosko, *Rheology Principles, Measurements, and Applications*, Wiley VCH, New York, 1994.

- [59] A. Oztekin and R.A. Brown, Instability of a viscoelastic fluid between rotating parallel disks: analysis for the Oldroyd-B fluid, *Journal of Fluid Mechanics*, **255** (1993), 473-502.
- [60] L. Schouveiler, P.L. Gal and M.P. Chauve, Instabilities of the flow between a rotating and a stationary disk, *Journal of Fluid Mechanics*, **443** (2001), 329-350.
- [61] R.W.G. Shipman, M.M. Denn and R. Keuningst, Free-surface effects in torsional parallel-plate rheometry, *Industrial & Engineering Chemistry Research*, **30** (1991), 918-922.
- [62] M. Lygren and H.I. Andersson, Turbulent flow between a rotating and a stationary disk, *Journal of Fluid Mechanics*, **426** (2001), 297-326.
- [63] R.W. Fox, A.T. McDonald and P.J. Pritchard, *Introduction to Fluid Mechanics*, John Wiley & Sons, Hoboken, NJ, 2004.
- [64] J. Ando, H. Nomura and A. Kamiya, The effect of fluid shear stress on the migration and proliferation of cultured endothelial cells, *Microvascular Research*, **33** (1987), 62-70.
- [65] L.A. Oliveira, J. Pecheux and A.O. Restivo, On the flow between a rotating and a coaxial fixed disc: numerical validation of the radial similarity hypothesis, *Theoretical and Computational Fluid Dynamics*, **2** (1991), 211-221.
- [66] M. Papadaki and L.V. McIntire, Quantative Measurements of shear-stress effects on endothelial cells, *Tissue Engineering Methods and Protocols*, **18** (1999), 577-593.
- [67] S.A. Safran, N. Gov, A. Nicolas, U.S. Schwarz and T. Tlusty, Physics of cell elasticity, shape and adhesion, *Physica A*, **352** (2005), 171-201.
- [68] Y.-B. Lu, K. Franze, G. Seifert, C. Steinhilber, F. Kirchhoff, H. Wolburg, J. Guck, P. Janmey, E.-Q. Wei, J. Kasch and A. Reichenbach, Viscoelastic properties of individual glial cells and neurons in the CNS, *Proceedings of the National Academy of Sciences*, **103** (2006), 17759-17764.
- [69] D.D. Deligianni, N.D. Katsala, P.G. Koutsoukos and Y.F. Missirlis, Effect of surface roughness of hydroxyapatite on human bone marrow cell adhesion, proliferation, differentiation and detachment strength, *Biomaterials*, **22** (2001).
- [70] D.L. Elbert and J.A. Hubbell, Surface treatments of polymers for biocompatibility *Annual Review of Material Science*, **25** (1996), 365-394.

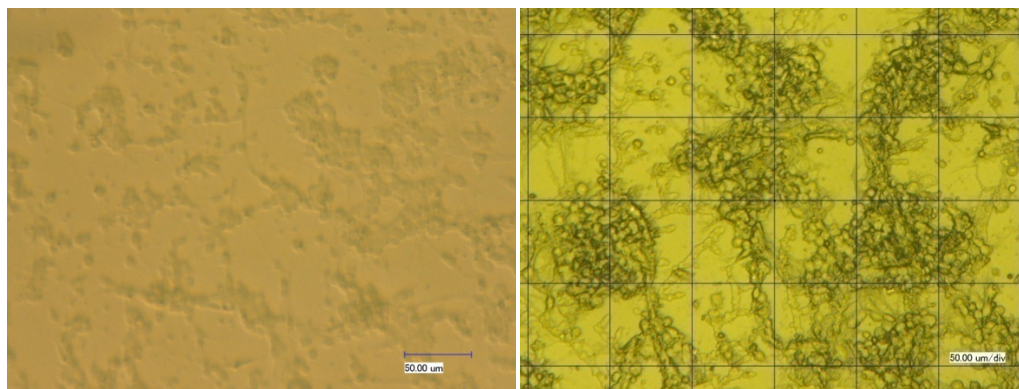
- [71] E. Eisenbarth, J. Meyle, W. Nachtigall and J. Breme, Influence of the surface structure of titanium materials on the adhesion of fibroblasts, *Biomaterials*, **17** (1996).
- [72] R. Ribeiro, P. Asthana, S. Ingole, B. Shi, T. Kuhn and H. Liang, Exploring surface texture for cell adhesion, *Journal of ASTM International*, **2** (2005), 1-6.
- [73] R. McMillan, B. Meeks, F. Bensebaa, Y. Deslandes and H. Sheardown, Cell adhesion peptide modification of gold-coated polyurethanes for vascular endothelial cell adhesion, *Journal of Biomedical Materials Research*, **54** (2001), 272-283.

APPENDIX A

Images taken before and after testing for chick embryo neuron cells on poly-D-lysine coated glass. These images demonstrate no cell shape and density before and after testing.



S15_10 chick embryo neuron cells on poly-d-lysine coated glass. Image before testing (left) and image after testing (right).



S16_25 chick embryo neuron cells on poly-d-lysine coated glass. Image before testing (left) and image after testing (right).

VITA

Aracely Rocha received her Bachelor of Science degree in mechanical engineering from The University of Texas-Pan American in 2006. She entered the mechanical engineering program at Texas A&M University in August 2006 and completed her M.S. in mechanical engineering in December 2008. She plans to continue at Texas A&M University to pursue the Doctorate degree in mechanical engineering. She has completed three out of six courses towards the doctorate degree and passed the Ph.D. qualifying exams in fulfillment of the Doctorate degree requirements in mechanical engineering in the areas of materials and heat transfer.

Her research interests include the fields of biomaterials and biocompatibility and to improve incorporation of implants into the body.

Ms. Rocha may be reached at:

Address: 3123 TAMU College Station, TX 77843-3123

Email Address: aracelyr1@msn.com

Education: B.S., Mechanical Engineering, The University of Texas-Pan American, 2006.

M.S., Mechanical Engineering, Texas A&M University, 2008.